CHALMERS
UNIVERSITY OF TECHNOLOGY

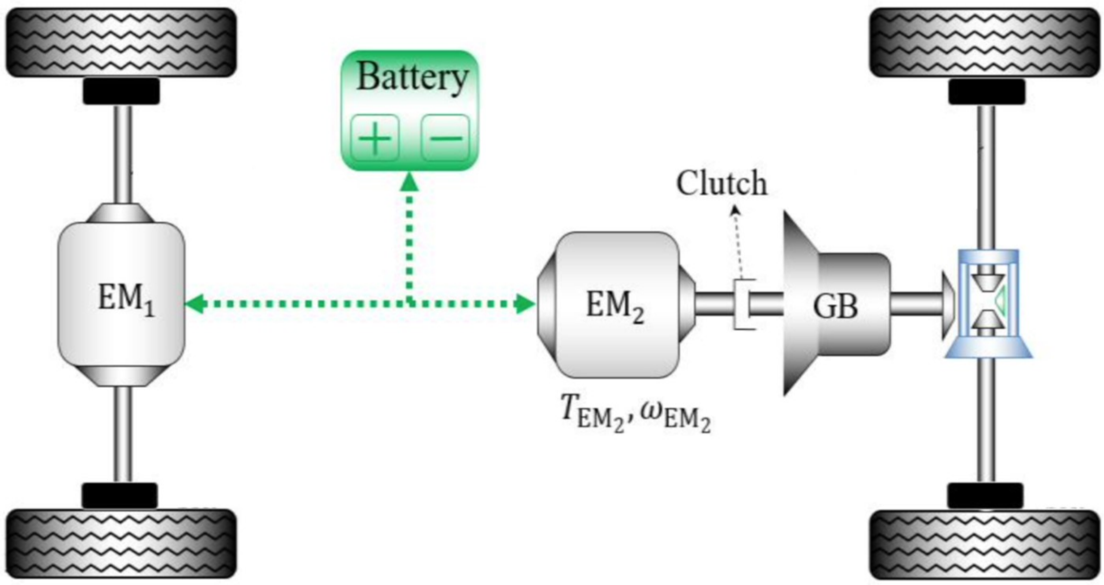

Optimal torque split strategy for BEV power-train considering thermal effects

Master's thesis in Automotive Engineering

AVANISH RAJ

DEPARTMENT OF ELECTRICAL ENGINEERING
CHALMERS UNIVERSITY OF TECHNOLOGY
Gothenburg, Sweden 2021
www.chalmers.se

Master's thesis 2021

Optimal torque split strategy for BEV powertrain considering thermal effects

AVANISH RAJ

Department of Electrical Engineering

Chalmers University of Technology
Gothenburg, Sweden 2021

Optimal torque split strategy for BEV powertrain considering thermal effecrs
AVANISH RAJ

This work is done in collaboration with Dhananjay Yadav from Vehicle Engineering, KTH Royal Institute of Technology, Stockholm.

Academic supervisor: Anand Ganesan, Industrial PhD student, Volvo Cars
Industrial supervisor: Shemsedin Nursebo Salih, Volvo Cars
Examiner: Prof. Sebastien Gros, Department of Electrical engineering

Master's Thesis 2021
Department of Electrical Engineering
Division of Systems and Control
Chalmers University of Technology
SE-412 96 Gothenburg
Telephone +46 31 772 1000

Cover: Powertrain architecture of battery electric vehicle with electric machines on both axles. The front electric machine has a clutch which can be used to disconnect the motor to save magentic drag losses.

Typeset in LaTeX
Printed by Chalmers Reproservice
Gothenburg, Sweden 2021

Optimal torque split strategy for BEV powertrain considering thermal effects
Avanish Raj
Department of Electrical Engineering
Chalmers University of Technology

Abstract

A common architecture for electric vehicles is to have electric machines on both the front and rear axle. This work is an attempt to derive an optimal torque split strategy between the two machines to reduce the overall energy consumption. A clutch is implemented on the front axle and its engagement is dynamically controlled to reduce the magnetic drag losses. With cluth disengaged, the entire torque will be delivered by a single machine and it can get quickly heated up. As electric machine and inverter losses are also dependent on temperature, a power loss map based on torque, machine RPM and temperature is considered. An upper temperature limit for both electric machine and inverter is imposed for component protection. Thermal models for electric machine, inverter and coolant circuit are simplified using system identification and model order reduction approach.An optimal torque split is created by minimising the energy loss over the entire drive cycle. Dynamic programming is used to investigate the benefits of including thermal losses and to generate an benchmark solution for optimal torque split strategy. Further, two online controllers are developed, one based on non-linear model predictive control and the other being a static controller with added heuristic rules to prevent temperatures of critical components to exceed the limits. A high-fidelity plant model was developed using VSIM as master and GT-Suite thermal model as slave to compare the performance of these controllers.

The results shows that it is possible to obtain decent thermal performance of electric motor and inverter with one node lumped parameter thermal model and a five node lumped parameter thermal model for the coolant circuit. Including thermal dynamics in the controller can constraint the temperature within the limits and give an optimal torque split. The benefit of adding temperature dependent thermal maps is found to be limited to certain operating regions and is not that significant for the powertrain configuration analysed in this report.The static controller with torque split based on instantaneous power loss also performed well for this configuration. The major contribution to energy saving was obtained by dynamic disengagement of clutch in the form of reduced magnetic drag losses.

Keywords: Optimal torque-split control strategy, battery electric vehicles, thermal model of electric machines, system identification, model order reduction, co-simulation.

Acknowledgements

We would like to thank our supervisors Anand Ganesan, Shemsedin Nursebo Salih and Andreas Andreasson from Volvo Car Corporation without whose constant support and guidance this thesis work would not have been possible. Special thanks to Ole-Fredik Dunderberg, our Energy Efficiency team manager at VCC, for seamless on-boarding and arranging a powerful computer when we needed more computation power for co-simulations. Our sincere gratitude to examiners, Prof. Sebastian Gros from NTNU and Prof. Mikael Johansson from KTH, for valuable suggestions and feedback.

Avanish Raj and Dhananjay Yadav, Gothenburg, June 2021

Contents

List of Figures

List of Tables

1
Introduction

The last few years has seen an increasing demand of battery electric vehicles (BEV). They have a more efficient powertrain as compared to an internal combustion engine vehicle (ICE) [1]. The energy is stored in batteries. Lithium-ion cells (Li-ion) are leading the charge for electrification. But still the energy density of Li-ion batteries is much lower than that of fossil-fuel. Thus even with a higher efficiency powertrain, the overall range of the vehicle is limited. In order to get acceptable range, vehicle manufacturers are installing bigger batteries in their vehicles. Manufacturing batteries for electric vehicles is an energy intensive process and emits a lot of CO_2 during its production.The raw materials required for battery manufacturing are also sourced by geographical reasons where there is a concern for human exploitation [2]. There is an increasing effort to use renewable energy for battery manufacturing and find battery chemistry which requires less exploitative materials like Cobalt. With usage of an electric vehicle in a location where the energy mix is predominantly through renewable sources, BEV can be a sustainable transport solution.

Since vehicle range is an important aspect for BEV, a lot of effort is put to improve the range through smart control strategies. Optimising energy distribution between different actuators, balancing the energy spent between propulsion and auxiliary demands, understanding driver behaviour linked with excessive energy consumption and providing coaching for economic driving are some strategies which have attracted heavy research [3][4]. Usually BEV have two or more motors, and optimal split of torque between the different machines can be done to save some energy. This kind of approach has been widely researched on hybrid vehicles and controllers with different complexities have been proposed [5][6]. In the present work, a dynamic torque split strategy between two electric machines has been proposed. This is investigated with regards to energy consumption for different drive cycles.

1.1 Background

The electric motors in a BEV are directly connected to the axles with a fix gear in between. The torque split between the machines is governed by rule based strategies. These strategies are optimised for some drive cycles but are not optimal for every driving condition. A study was done previously by Chalmers and Volvo [7], where the benefit of adding clutch on the front axle motor was investigated. Two configurations were considered – with clutch and without clutch. The vehicle configuration used is shown in figure 1.1.

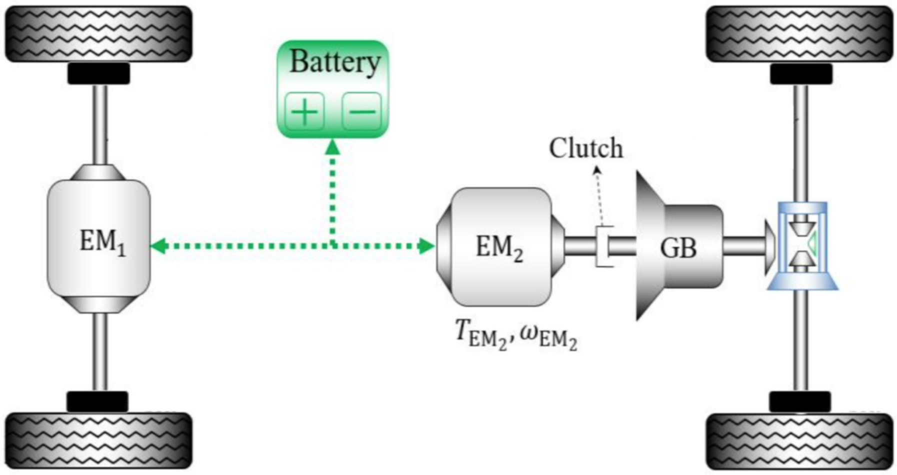

Figure 1.1: Vehicle architecture with two electric machines and clutch on front axle

In both the cases a dynamic torque split was done to reduce the instantaneous energy consumption. Figure 1.2 shows the benefit that can be achieved with including clutch and dynamically controlling clutch engagement and disengagement. This benefit is observed with clutch disengaged as the magnetic drag losses are prevented when the front motor is not spinning.

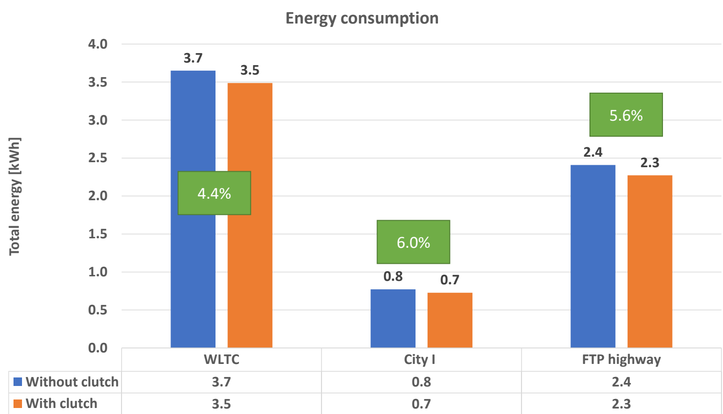

	WLTC	City I	FTP highway
Without clutch	3.7	0.8	2.4
With clutch	3.5	0.7	2.3

Figure 1.2: Energy consumption with and without clutch for instantaneous torque split strategy

It was observed that for obtaining energy benefit, the controller disengaged the clutch. The percentage of drive cycle driven only on rear machine varied with the cycle type and the load requirements. The project was started by implementing this static controller, which gives a dynamic torque split based on instantaneous power loss, on our chosen powertrain configuration.Apart from energy benefits, the temperature of electric machine and inverter was of interest. It was hypothesized that since a single machine would be running for quite some time, it can get heated quickly and the temperature limits can be exceeded. The electric machine and inverter temperatures are constrained to an upper maximum limit for component protection. In the case of electric machine, end-winding temperature is of prime concern, as it generally reaches highest temperature and continuous operation at high temperature can lead to insulation degradation [8]. For inverter, the IGBT temperature is of interest [9]. These temperatures are also monitored in the vehicle. Figure 1.3 shows the result for the same for a custom city drive cycle.

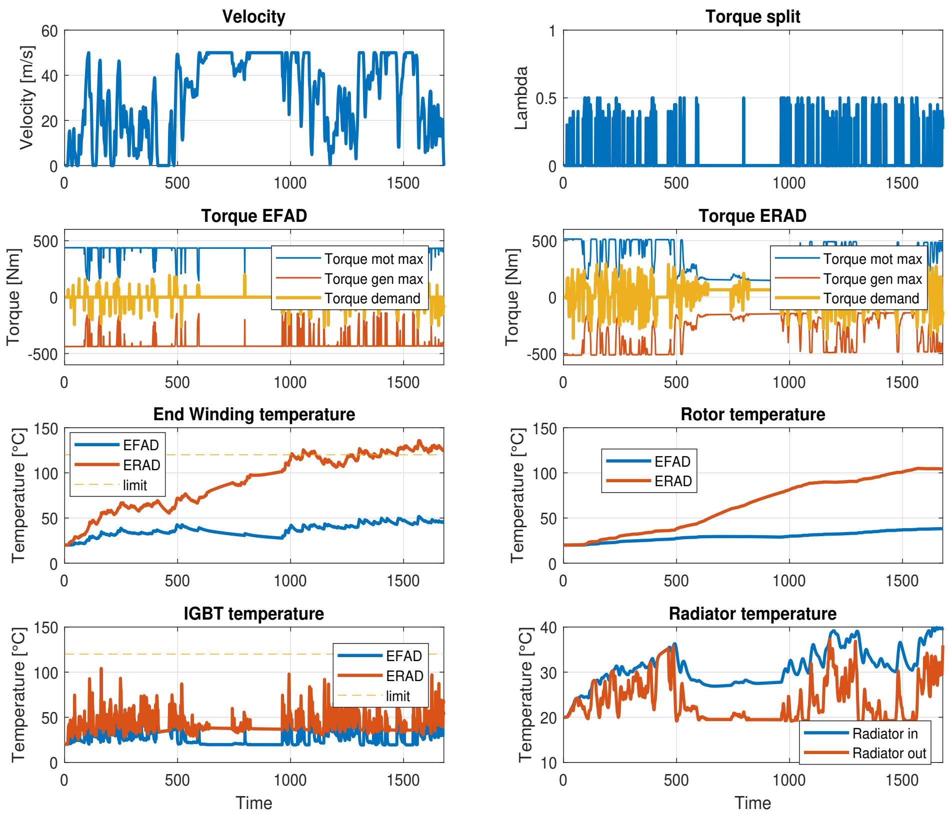

Figure 1.3: Energy consumption with and without clutch for instantaneous torque split strategy

Lambda (λ) represents the fraction of total torque delivered by the front electric machine. $\lambda = 0$ implies the entire torque is delivered by the rear machine and the clutch is disengaged. $\lambda = 1$ represents entire torque delivery by the front machine. As shown by the figure 1.3, after 1500 seconds the temperature of end-winding has exceeded the safe operation limit.The IGBT temperature is within the limit for this case. This was possible as the controller does not have any indication of the thermal behaviour of the components. Thus, there is a need of building a controller which provides dynamic torque split keeping the temperature of components within limits. The temperature dependance on efficiency should also be considered.

1.2 Scope

The scope of the project is to build an optimal vehicle supervisory controller for a BEV which can dynamically split the torque between the two electric machines and control the clutch actuation to minimise the overall energy consumption while meeting the propulsion and thermal demands. The project scope has three distinct requirements- build control oriented thermal models, implement optimal dynamic controllers, and build a high fidelity plant model to verify the controller. The project scope is divided into specific objectives which are shown below–

1. Build control oriented thermal models for electric machine, inverter and the complete coolant circuit
2. Formulation of the optimal control problem
3. Create a high-fidelity plant model including thermal dynamics, clutch, rotational and longitudinal dynamics
4. Implement dynamic programming to obtain a benchmark solution and verify the effect of considering thermal dynamics
5. Implement an online controller and verify its performance against benchmark

1.3 Limitations

The controller is designed for a vehicle architecture as shown in figure 1.1. The electric machine used on front and rear axle are specified by Volvo Cars as per their project requirement. The coolant circuit is simplified to just the electric drive circuit. The conclusion regarding the behaviour of the controller are derived based on this particular powertrain architecture. Verification of the controller is done in a virtual environment.

1.4 Outline

This section presents the outline for the entire report to guide the reader. In chapter 1, the motivation for the project is explained. In chapter 2, the theory required to understand the methods is given in a brief manner. Chapter 3 describes how the different objectives were achieved. Results and discussions are presented in chapter 4. Final conclusions and future expansions to the project are summarized in the chapter 5.

2
Theory

The work of designing a controller for any purpose can be mainly divided in three parts as listed below-

1. Creating a plant model
2. Creating controller models
3. Formulating the optimal control problem and implementing the controller

Plant models are used to verify the performance of the controllers and to understand their behaviour in the real vehicle. The plant model thus needs to closely follow the behaviour of the actual vehicle. The theory section gives an overview to the different modeling environments used to create the high-fidelity plant model for our application.

In order to reduce the computation time required by the controllers the component model needs to be simplified. The performance of the controller depends both on the accuracy of the simplified models and the architecture of the controller itself. The section presents two ways of model simplification– system identification and model order reduction. Some background information about optimal control problems and different types of controllers are also presented.

2.1 Modeling environment

2.1.1 VSIM

VSIM is an Volvo developed tool, based on MATLAB/Simulink, used for virtual verification of complete vehicles. It captures the mechanical, electrical and thermal energy flow throughout the vehicle. It is mainly used for predicting the energy consumption, vehicle performance, component dimensioning, control software calibration and for load case generation[10]. It uses high-fidelity analytical models of different components arranged as per the vehicle concept. The simulation environment is divided in three main parts- Environment, Driver and the Vehicle as shown in the figure 2.1. The environment module provides the road conditions,the ambient temperature,pressure,humidity, the wind speed in different directions etc. It provides data to both the driver and the vehicle module. The driver module can model different driver behaviours and outputs mainly the accelerator, brake and the clutch pedal positions. The positions can be calculated in order to follow a particular drive cycle also. The vehicle module is further divided in two units the plant and the controller. The plant contains the models for different components including the electric machines, inverters, transmission, driveline,brakes, wheels, chassis, HV

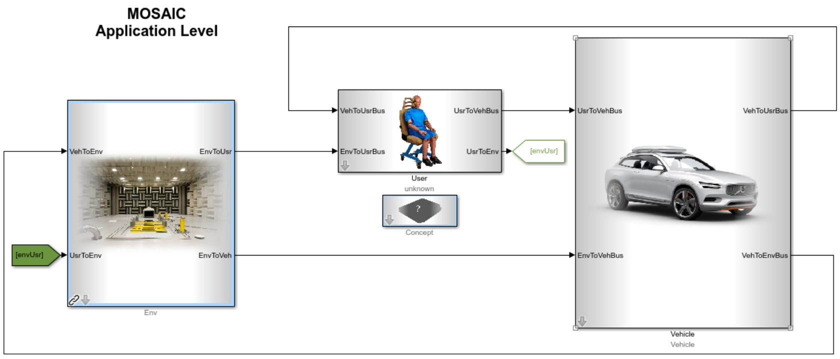

Figure 2.1: VSIM simulation environment

system, battery, LV system etc. Figure 2.2 shows a typical plant model. Different components are actuated according to the individual controller signals. The torque split is decided by a vehicle supervisory controller.

2.1.2 CVTM

CVTM or the complete vehicle thermal model is a 1D system level modeling of the entire thermo-fluidic domain of the vehicle in GT-suite. The coolant harness for different vehicles are modeled along with component heat generation for electric machines, inverters, batteries etc. A control system is also modeled which governs the opening of different valves and pump speeds. Heat is transferred from the different components to the coolant which is pumped to the air cooled radiator. The AC system and chiller/heater system for the battery is also modeled. Figure 2.3 shows a typical thermal circuit for the vehicle.

2.2 Component models

2.2.1 Behaviour and thermal modeling of electric machine

An electric machine provides the traction torque in an battery electric vehicle. The electric machine converts the electrical energy from battery cells to mechanical energy. In essence, it is an energy converter which is more efficient than an internal combustion engine.
Fig. 2.4 shows the torque-speed characteristic of the electric machine considered in this study. At lower speeds, the machine can provide constant maximum torque right from zero speed. At higher speeds, the power limit is reached and torque decreases hyperbolically. Fig. 2.4(a) depicts the variation of torque limit with different temperatures. At higher temperatures the max torque delivered by the machine reduces as the magnets in rotor become weaker. Similar behavior is seen in variation with battery voltage, shown in 2.4(b). As the battery voltage reduces, the torque limit at higher speeds reduces.

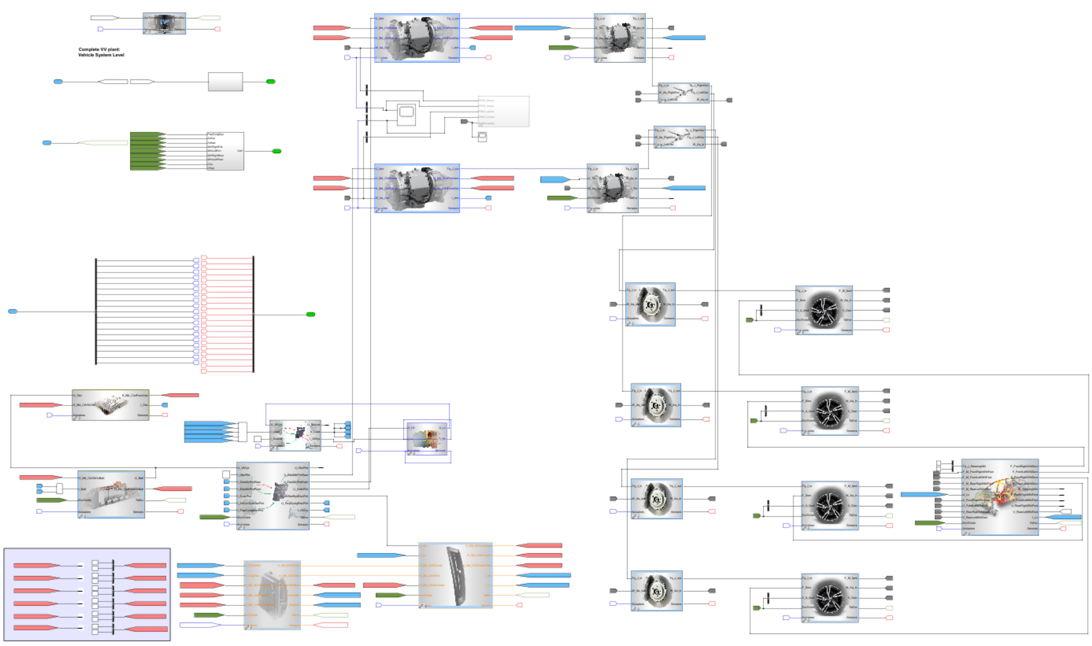

Figure 2.2: The vehicle plant model inside VSIM

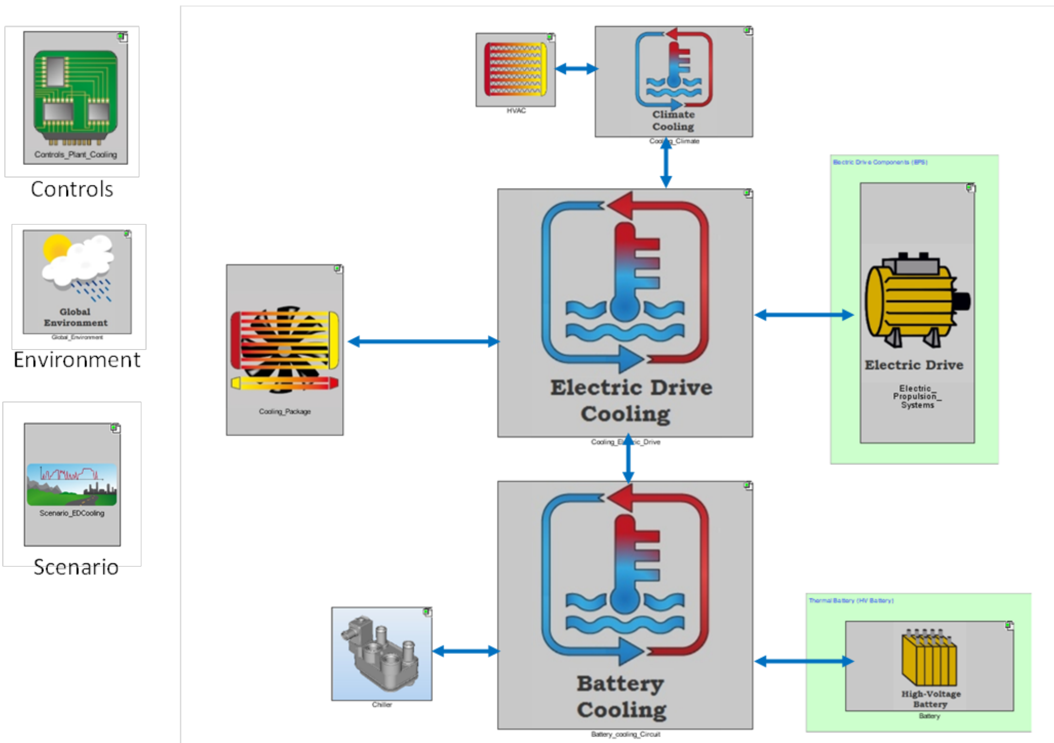

Figure 2.3: Complete vehicle thermal model in GT Suite

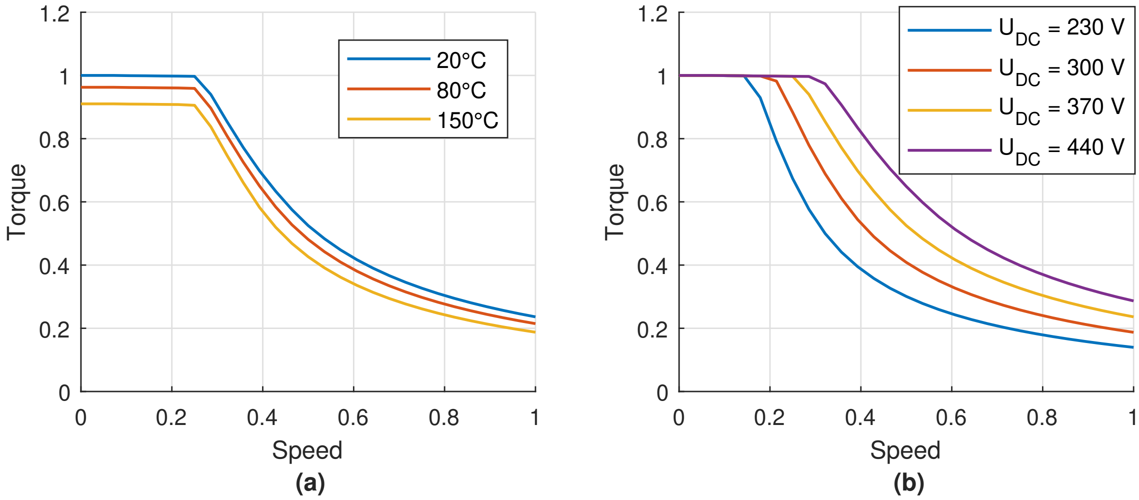

Figure 2.4: Electric machine torque limit variation with (a) temperature and (b) battery voltage (normalized axis).

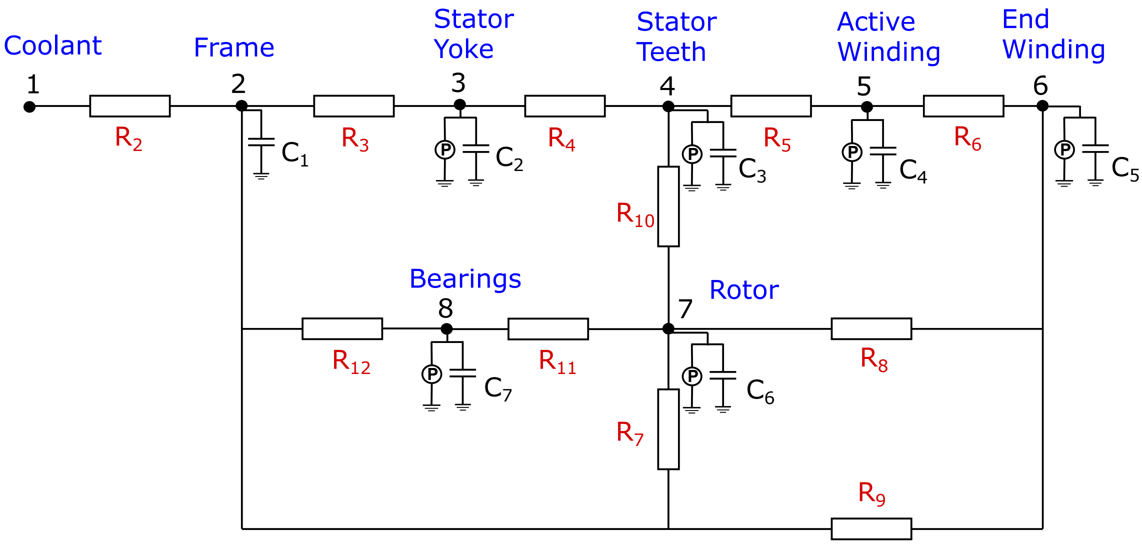

Figure 2.5: Electric machine thermal network

Fig. 2.5 depicts the equivalent thermal network model of an electric machine. The different components of an electric machine are represented by nodes. The power loss in the form of heat (represented by P) in these components are lumped at the nodes. Likewise the thermal capacities (represented by C) of the components are lumped. The thermal resistance for heat flow in between these components is represented by R. The derivation of this thermal network can be found in details in [11] and [12]. Using the thermal network, the temperatures at nodes can be obtained by the following transient heat transfer equation.

$$\mathbf{C}\frac{d}{dt}(\mathbf{T}) = -\mathbf{G}\mathbf{T} + \mathbf{P} \tag{2.1}$$

where $\mathbf{T}$ is the node temperature vector, $\mathbf{P}$ is the power loss vector, $\mathbf{G}$ is the thermal conductance matrix and $\mathbf{C}$ is the diagonal thermal capacitance matrix.

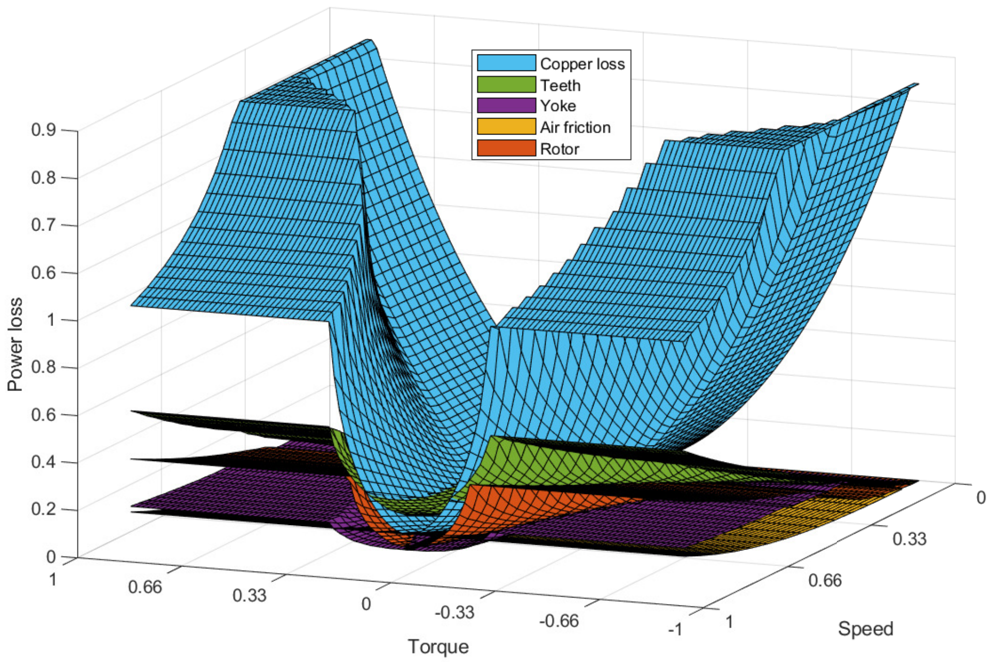

Figure 2.6: Electric machine losses from different source (normalized axis)

Fig. 2.6 shows the relative contribution from different components to electric machine losses. It can be seen that copper loss due to Joule heating in winding has the major contribution. The torque is proportional to current and copper loss is proportional to current squared. Hence, we see that the copper loss is parabolic in torque. The losses in teeth, yoke and rotor are iron losses due to magnetically induced eddy currents. It is important to note that the magnetically induced losses increase with speed even at zero torque. This is the source of magnetic drag loss which makes it necessary to include clutch to decouple the electric machine from wheels when it is not delivering torque.

The losses from electric machine depend on temperature and battery voltage as well which are relevant for this study. Fig. 2.7(a) shows the variation of total power loss of electric machine with temperature. It can be observed that the losses increase with increase in temperature at lower speeds and reduce at higher speeds. At lower speeds, the contribution due to copper loss dominates iron losses. With increase in temperature, the resistivity of winding increases causing copper losses to increase. At higher speeds the magnetically induced iron loss dominates. The magnetic strength of magnets reduces at higher temperature. Hence, we observe that total power loss reduces with increase in temperature at higher speeds.

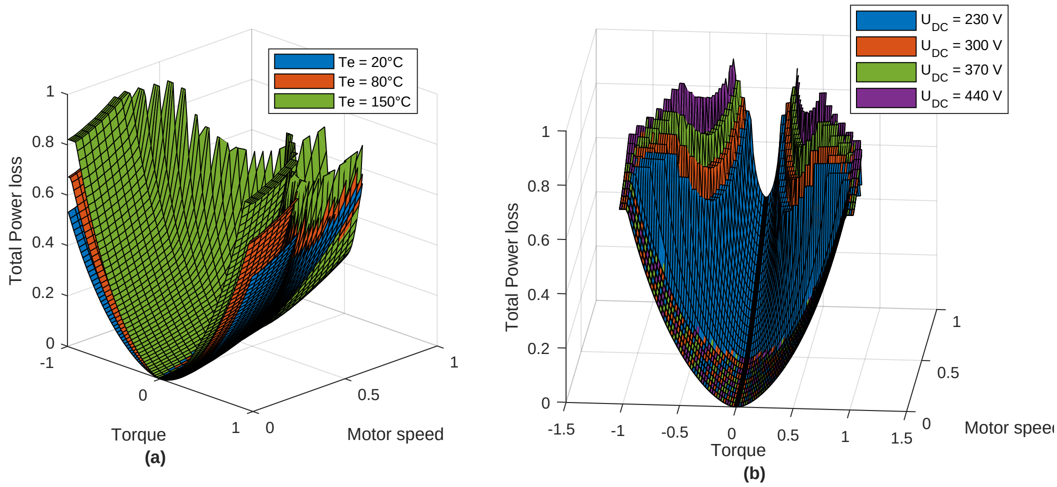

Figure 2.7: Electric machine loss map variation with (a) temperature and (b) battery voltage (normalized axis)

Figure 2.7(b) illustrates the total power loss map of electric machine at different battery voltages. We observe that blue plot is predominant indicating higher power loss at low battery voltage. The electric machine will draw more current at lower voltages to deliver the power required corresponding to a given torque and speed combination. Hence, the copper losses increase at lower battery voltages.

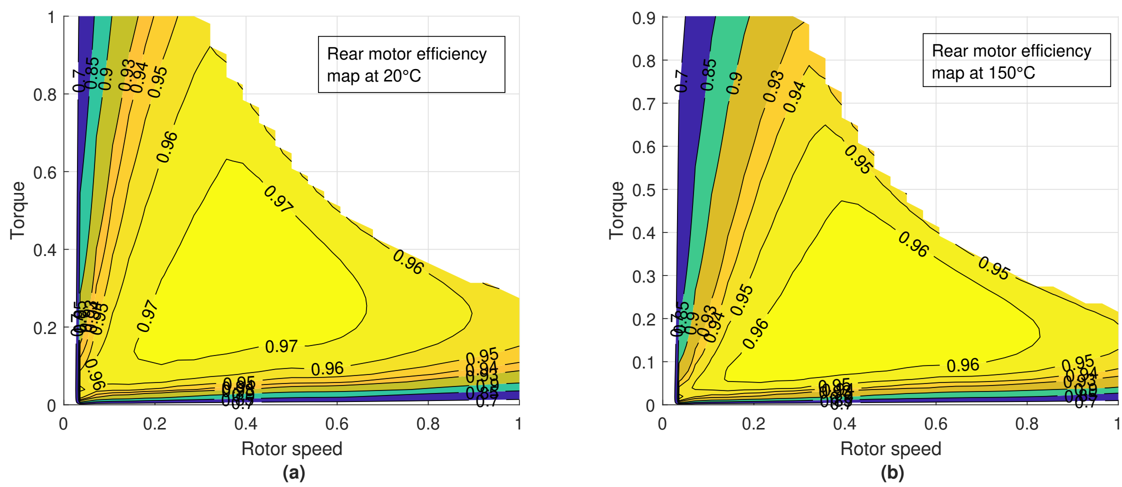

Figure 2.8: Efficiency map of electric machine at (a) 20°C and (b) 150°C

Since the power loss of electric machine varies with temperature, the efficiency also changes with temperature. Fig. 2.8 shows the efficiency map of electric machine at two temperatures: 20°C and 150°C. We can observe that the maximum efficiency reduced from 0.97 to 0.96 as temperature increased from 20°C to 150°C. This happens because of increase in copper losses as resistivity of winding increases with temperature. Also, we notice that the iso-efficiency contours deflate towards higher rotor speed as temperature increases. This is due to the reduction in iron losses as magnets become weaker at higher temperature.

2.2.2 Behaviour and thermal modeling of inverter

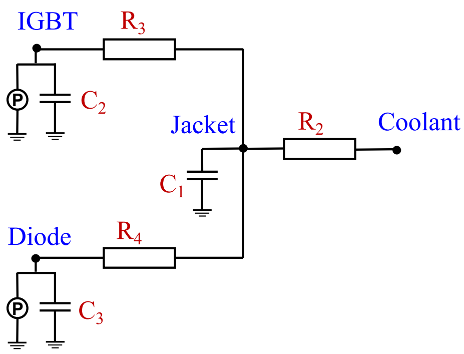

Figure 2.9: Inverter thermal network

Inverter converts the DC current from battery to AC in motor mode and AC current from electric machine to DC in generator mode in case of regenerative braking. Inverter has power electronic components such as IGBT and diodes which handle high amount of power. Even a small voltage drop across these components at high currents amounts to significant power loss in the form of heat. Fig. 2.9 depicts the thermal network of the inverter. The heat from IGBT and diode is carried to the inverter jacket, from where it is rejected to the coolant. Equation 2.1 is used to find the temperature at nodes.

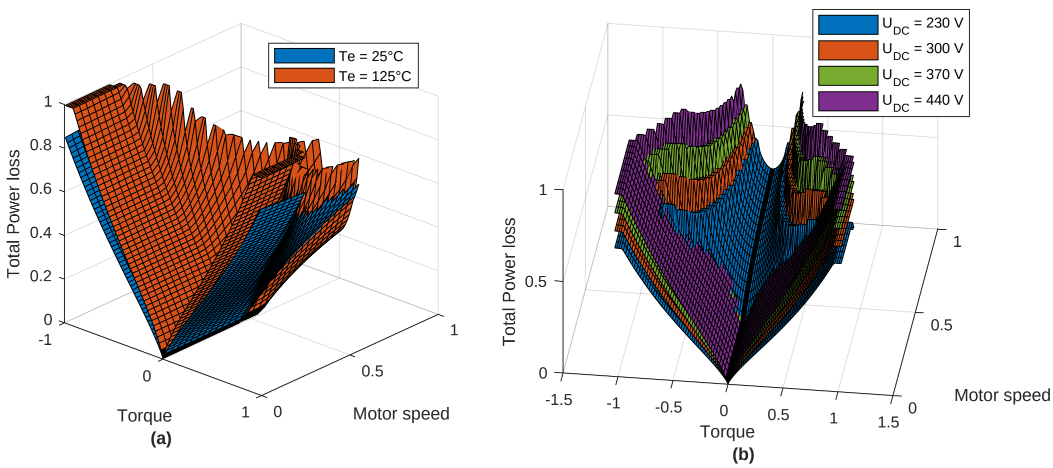

Figure 2.10: Inverter loss map variation with (a) temperature and (b) battery voltage (normalized axis)

Similar to electric machine, the total power loss from inverter also varies with temperature and battery voltage. Fig. 2.10(a) shows the total power loss map of inverter at two temperatures. We see that at higher temperature the power loss is more. Fig. 2.10(b) depicts the total power loss at different voltages. At lower speeds, the total power loss is more for higher voltage and at higher speeds the power loss is more for lower voltage.

2.2.3 Vehicle cooling system model

Heat generated by the electric machines and the inverters are transferred to the coolant in the cooling jacket. The coolant is then cooled by passing it through a air cooled radiator. An electric pump is used in the circuit to maintain the desired flow rate. Electric pump power consumption is a function of the coolant mass flow rate. The cooling circuit model used in this study is shown in the figure 2.11.

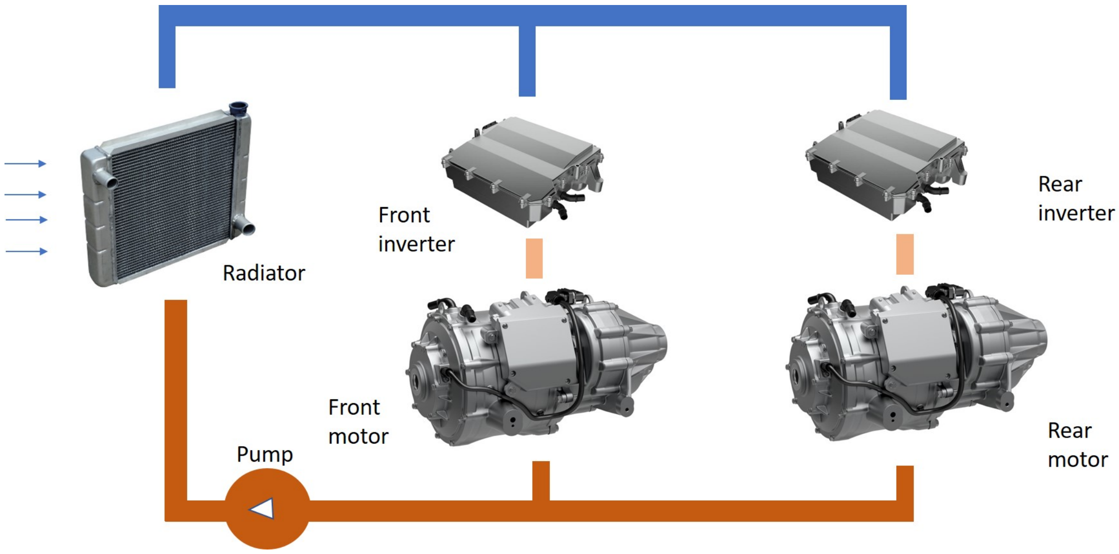

Figure 2.11: Electric drive coolant circuit

2.3 Model simplification techniques

Two widely used methods to simplify models for control application are System Identification and Model order reduction. This section gives a brief introduction to both these methods.

2.3.1 System Identification

System identification is a method of building mathematical models based on measurement of system input and output signals. A series of known input signals is passed through the plant model and the outputs are recorded. The plant model is approximated to a simple model and then its parameters are tuned to give a good enough match for the control application. The steps involved in system identification are [13]-

1. Observe the response of the system when it is excited by simple input signals (example- Step input, impulse function)
2. Based on the previous system knowledge or the response of the system select a model to approximate system behaviour
3. Calibrate the model parameters by minimising the error between the actual output and the simulated signal
4. Validate the simplified model against different test cases

It is important to note that the models obtained from system identification are useful only for specific applications and should not be treated as a alternative to system physical models.

2.3.2 Model order reduction

In general sense, model order reduction refers to reducing the computational complexity of a mathematical model. Here, we use a more precise definition of model order reduction in the context of control theory [14]. Given a dynamic system with n states:

$$G : \begin{cases} \dot{x}(t) = f(x(t), u(t)), & x(t) \in \mathbb{R}^n, u \in \mathcal{U} \\ y(t) = g(x(t), u(t)) \end{cases} \tag{2.2}$$

find a system with r states:

$$G_r : \begin{cases} \dot{z}(t) = f_r(z(t), u(t)), & z(t) \in \mathbb{R}^r, u \in \mathcal{U} \\ y_r(t) = g_r(z(t), u(t)) \end{cases} \tag{2.3}$$

such that $r < n$ and error $||y - y_r||$ is under a predetermined limit.
The computational complexity of dynamic systems is atleast proportional to the order n. In optimal controllers such as LQR, where Riccati equation is solved, the computation time is proportional to cube of order n^3. For benchmark analysis like dynamic programming, the computations are proportional to exponential in order p^n. Hence, model order reduction can save a lot of computation time by finding system with fewer states while still capturing the system output to a certain level of accuracy.

2.4 Optimal control problem

A dynamic system is defined as a system which depend both on the existing state values and the control action applied. Optimal control problem deals with finding a set of control inputs which can minimise a cost function over a certain period of time, while following all the state and control constraints. Let,

- $X = [x_1, x_2 ... x_n]'$ denote a state vector
- $U = [u_1, u_2 .. u_m]'$ denote a control vector
- $f(X, U) = 0$ denote a general dynamic system
- $g(X, U) = 0$ denote the set of equality constraints
- $h(X, U) > 0$ denote the set of inequality constraints
- $L(X, U) = 0$ represents a cost function
- $\Phi(X(t_f), t_f)$ is the terminal cost

and,

$$J(U) = \Phi(X(t_f), t_f) + \int_{t_0}^{t_f} L(X, U)\, dt \tag{2.4}$$

Then the optimal control problem is defined as

$$\min_U J(U) \tag{2.5}$$

such that

$$f(X, U) = 0$$
$$g(X, U) = 0$$
$$h(X, U) > 0$$

2.5 Controller

2.5.1 Dynamic Programming

Dynamic programming (DP) is a numerical method to solve optimal control problems. It is able to provide optimal solutions to problems of any level of complexity. It can handle multiple constraints on both input and state side. The main disadvantage of DP is that it requires all the information to be known in advance. Thus it cannot be used as a real time online controller. Nevertheless, as it able to provide global optimal solution limited to the level of discretization, it can be used to give optimal performance benchmark [6].

It is based on the Bellman's principle of optimality which is stated as-
"An optimal policy has the property that whatever the initial state and initial decisions are, the remaining decisions must constitute an optimal policy with regard to the state resulting from the first decision [15]".

Consider a discrete time system

$$x_{k+1} = f_k(x_k, u_k) \tag{2.6}$$

where k takes numerical values 0,1,2...so on. x_k is the states of the system and u_k is the control action applied at time step k. The states and control are constrained such that $x_k \in X_k$ and where $u_k \in U_k$. Considering the control policy for N time steps to be

$$u = [u_0, u_1, u_2, ..., u_{N-1}]$$

the cost of the policy with the initial state x_0 can be written as

$$J(x_0, u) = L_N(x_N) + \sum_{k=1}^{N-1} Ł_k(x_k, u_k)$$

The optimal cost function can be obtained by

$$\min_u J(x_0, u)$$

which yields the optimal control policy as

$$u = [u_0^*, u_1^*, u_2^*, ..., u_{N-1}^*]$$

Considering now the sub problem of minimising the cost to go from time step i to N

$$Y(x_i, i) = L_N(x_N) + \sum_{k=i}^{N-1} L_k(x_k, u_k)$$

the optimal solution as per Bellman's principle can be given by $[u_i^*, u_{i+1}^*, ..., u_{N-1}^*]$. $Y(x_k, k)$ denotes the optimal cost to go from time step k to the end [15].

At any time instant, for a particular state, the application of control is usually associated with a cost proportional to the control action and the state itself. In a dynamic programming problem, which is based on bellman optimal principle, we first discretize the states and the control inputs for the entire time domain. Proceeding backwards in time, from time step N-1 to 1, we have the end cost

$$J_N = L_N(x_N)$$

which is just a function of state. The cost at each intermediate time step called cost-to-go can be calculated as

$$J_k(x_k) = \min_u (L_k(x_k, u_k) + J_{k+1}(f_k(x_k, u_k)))$$

where $L_k(x_k, u_k)$ represents the cost associated with the state and the control. Application of this control action will update the state to the next state which itself have its own cost-to-go. Cost-to-go basically represents the minimum cost that is required to go till the end time from that state. If $u_k^o = u_k^0(x_k)$ minimises the right hand side of previous equation for each x_k and k, then the policy determined by $[u_0^o, ..., u_{N-1}^o]$ is the optimal one [6].
Dynamic programming are based on discrete decision process and thus require the states and the control action to be discretized. Choosing a finer grid will improve the accuracy of the solution but will also increase the computational burden. The computational burden for a DP scales linearly with the problem time, but exponentially with the number of states and control inputs. For a problem with N time steps, n states with p discretization and m controls with q discretization the computational time will scale according to below equation [6].

$$\text{Computational time} \propto N \cdot p^n \cdot q^m$$

2.5.2 Model predictive control

Model predictive control (MPC) is a type of receding horizon optimal control which is used to control a process while minimizing cost and satisfying a set of constraints [16]. MPC predicts the system behavior in future timeslots based on system dynamic model and takes action which optimizes the cost over the time horizon. This predictive ability is the main advantage of MPC over traditional controllers like

PID. Even tough MPC calculates control actions over the finite horizon, only action at current time step is implemented and then the optimal control problem is again solved at next timestep based on updated system states. This takes care of any disturbances or shortcomings in the model.
A typical schematic of model predictive control can be represented as:

$$\begin{array}{lll} \underset{u_k}{\text{minimize}} & \sum_{k=0}^{T} \text{cost}(x_k, u_k) & \\ \text{subject to} & x_{k+1} = Ax_k + Bu_k & k = 0, \ldots, T, \\ & x_k \in \mathcal{X} & k = 0, \ldots, T, \\ & u_k \in \mathcal{U} & k = 0, \ldots, T \end{array} \tag{2.7}$$

where T is the time horizon, x_k are the states at time step k, u_k are the inputs, $\mathcal{X}$ is the bound on states, $\mathcal{U}$ is the bound on inputs and the first constraint is the linear state-space equation in discrete form.

3
Methods

3.1 Plant model

A high fidelity plant model is required to evaluate the performance of the controller and the model simplifications. Plant can be modeled in two types- backward model and forward model. The backward model takes in the drive cycle and calculates the torque requirement accordingly. The forward model employs a driver model which gives the accelerator and the brake pedal signals. These signals are dependent on the difference between the target velocity and the current velocity. This accounts for the rotational dynamics of the electric machines and the rotating components and also the longitudinal dynamics of the vehicle. Figure 3.1 and 3.2 shows the backward and forward model respectively.

The two plant model differs in the way the torque is calculated and the behaviour of the system during clutch engagement. In the forward model the, the electric motor control is done through a speed controller. This allows it to capture the torque jumps during clutch engagement/disengagement. The driver model uses vehicle velocity as feedback and adjusts the applied torque to always follow desired target speed. This can be a problem with backward model as any error in torque calculation (especially during clutch engagement/ disengagement) will lead to a deviation from the target velocity profile. Also, it cannot capture the torque jumps. The constant torque characteristic of backward model is useful when comparing different controller models. Table 3.1 lists the basic characteristics of both the models.

3.1.0.1 Co-Simulation with GT-Suite

VSIM thermal model captures the heat generation by the motor and inverter but lacks a proper coolant circuit model. The CVTM environment in GT-Suite has a detailed thermal model and incorporates the power loss models for electric machine and inverter. It also has a battery model. The CVTM needs the torque, rotor speed of the electric machines and the vehicle velocity as an input. In order to capture realistic thermal characteristics for the entire drive cycle a co-simulation environment was set up using Simulink as the master model and GT-suite CVTM as slave. For a given time instant, the torque/omega is calculated by the Simulink model and is passed to the GT-suite model as an input. The GT-suite model solves the thermal network and outputs the temperature of the motor,inverters and the radiator components. It also outputs the power loss from the electric machine, inverter and the pump. Summation of the power loss from the two electric machines, two inverters and the pump lead to the total power loss and when integrated gives the total energy loss for the cycle. Adding the mechanical power to the power losses, gives the total power consumed and its integration is the total energy consumed for the cycle.

Table 3.1: Characteristics of backward and forward model

	Backward model	**Forward Model**
Torque request	Done by calculating the force required to move the vehicle according to the velocity profile	Torque mapping according to accelerator pedal signal
Brake Request	Brake torque is calculated as the difference between torque requested and the minimum wheel torque that can be applied by the machines	Brake torque demanded as per brake signal by driver
Electric machine's RPM	Calculated according to vehicle velocity	Calculated from the forward dynamics of vehicle motion as per applied tractive torque
Effect of clutch engagement	RPM and torque both goes to zero. Torque request is reduced	RPM goes to zero. Electric machine has a speed controller which adjusts the torque accordingly. Driver takes corrective action to maintain speed
Electric machine power loss model	Look up table based on Torque, RPM, Voltage DC, Te_{rotor}, Te_{copper}, Te_{NDE}, Te_{DE}	Look up table based on Torque, RPM, Voltage DC, Te_{rotor}, Te_{copper}, Te_{NDE}, Te_{DE}
Inverter power loss model	Look up table based on Torque, RPM, DC voltage, Te_{rotor}, Te_{IGBT}, Te_{Diode}	Look up table based on Torque, RPM, DC voltage, Te_{rotor}, Te_{IGBT}, Te_{Diode}
Electric machine thermal model	8 node lumped parameter thermal model	8 node lumped parameter thermal model
Inverter thermal model	4 node lumped parameter thermal model	4 node lumped parameter thermal model

3.2 Controller models

In order to determine the torque split, the controller needs models for calculating the torque required by the vehicle for driving a particular velocity profile, the elec-

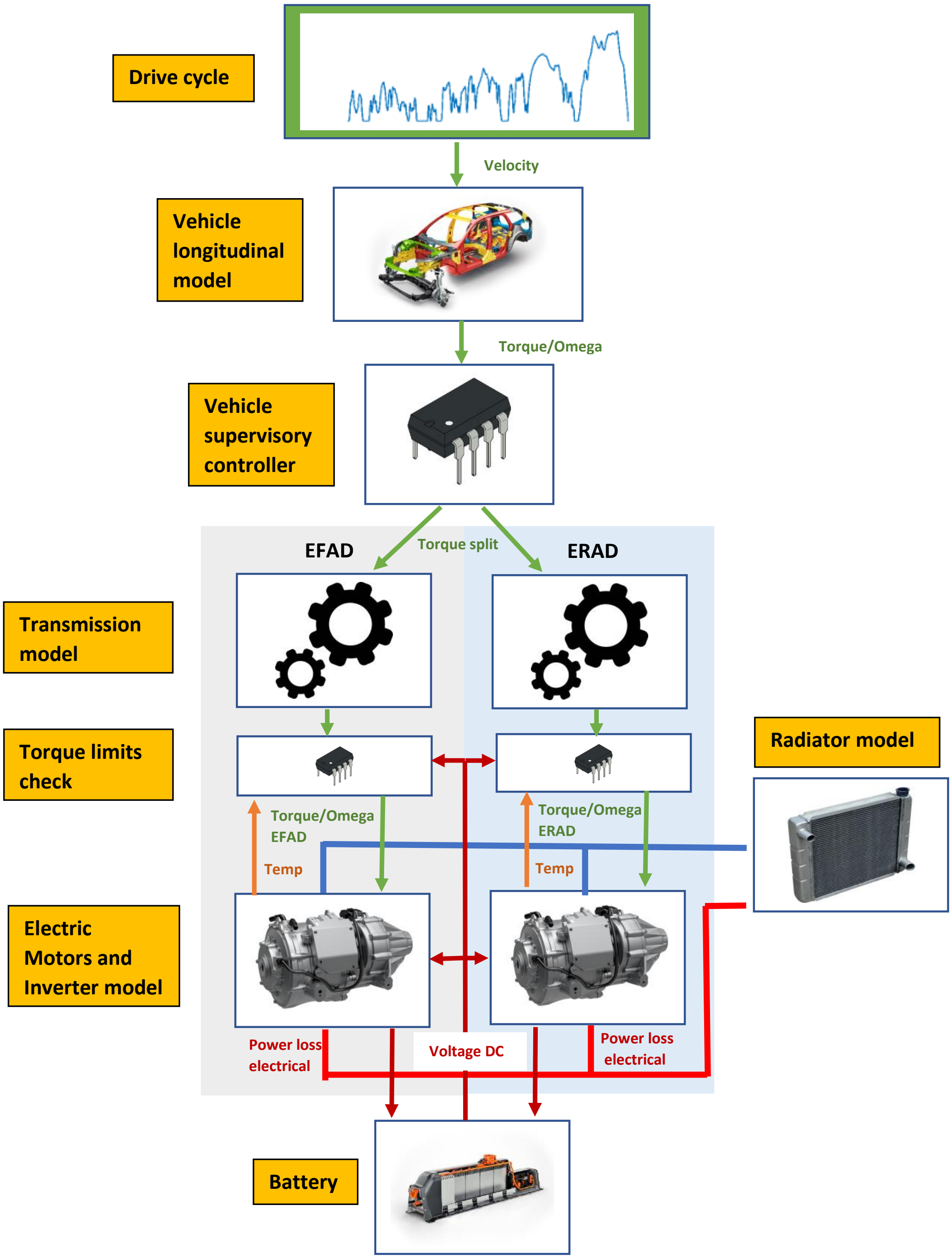

Figure 3.1: Backward modeling of plant

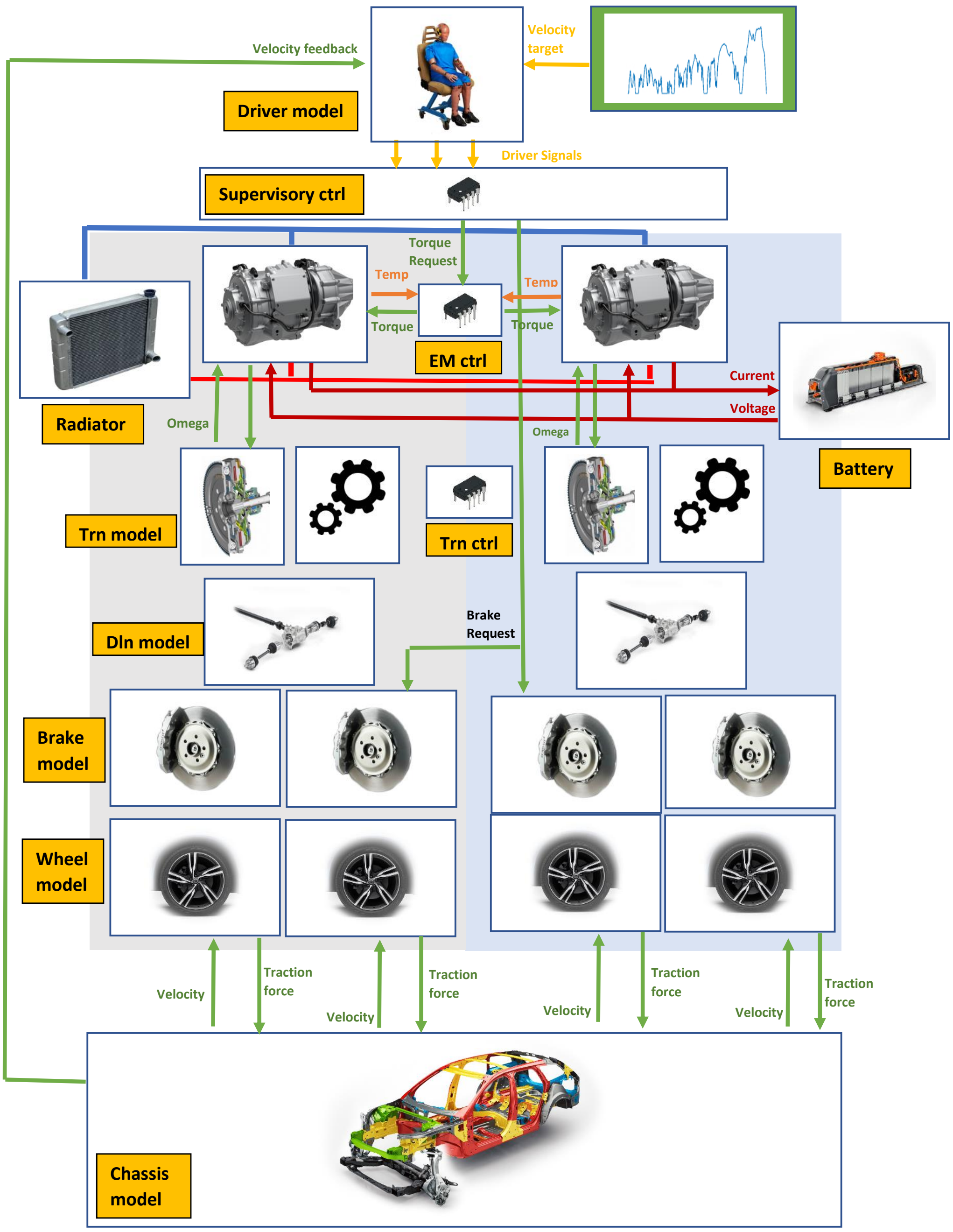

Figure 3.2: Forward modeling of plant

trical power loss of the machines, inverter and the pump losses. As explained in section 2.2.1, the power loss of electric machines are dependent on torque, omega, temperature of machine end-winding, rotor, and DC voltage. The inverter power loss are dependent on torque, omega, temperature of end-winding, rotor, IGBT, diode and DC voltage. There is also an upper thermal limit imposed on electric machine end-winding temperature and inverter IGBT temperature. The controller thus requires following models-

1. Torque calculation model
2. Cooling circuit model
3. Simplified thermal model
4. Power loss model for electric machine and inverter
5. A battery model calculating the state of charge(SOC) of the battery

3.2.1 Torque calculation model

The torque demanded by the vehicle to follow a particular drive cycle is calculated by equation

$$M_{req,Vehicle} = \left(\left(m+4\cdot\frac{J_{wheel}}{r_{wheel}^2}+\frac{J_{ERAD}}{(r_{wheel}\cdot diff_{rear})^2}+\frac{J_i}{(r_{wheel}\cdot diff_{front})^2}\right)\cdot\dot{v}+c_1\cdot v^2+c_2\cdot v+c_3\right)\cdot r_{wheel} \tag{3.1}$$

$$M_{brake} = M_{req,Vehicle} - (M_{EFAD,min})\cdot diff_{front} - (M_{ERAD,min})\cdot diff_{rear} \tag{3.2}$$

$$M_{min} = f(V_{DC}, \omega, T_{rotor}, T_{endwinding})$$

$$M_{traction} = M_{req,Vehicle} - M_{brake}$$

$$J_i = J_{em,front}/J_{front} \text{ for clutch engaged/disengaged}$$

where,
$M_{req,Vehicle}$ = torque required by vehicle to follow drive cycle,
M_{brake} = brake torque,
$M_{traction}$ = Traction torque,
m=mass of the vehicle,
J_{wheel} = Inertia of the wheel,
$J_{em,rear}$ = Inertia of the rear electric machine and transmission,
$J_{em,front}$ = Inertia of the front electric machine and transmission,
J_{front} = Inertia of front transmission,
$diff_{front}$ = gear ratio of front differential,
$diff_{rear}$ = gear ration of rear differential,
r_{wheel} = radius of the wheel,
v = vehicle velocity,
$\dot{v}$ = Vehicle acceleration,
c_1 = aerodynamic loss coefficient,
c_2 = velocity dependent rolling resistance coefficient,
c_3 = static rolling resistance coefficient.

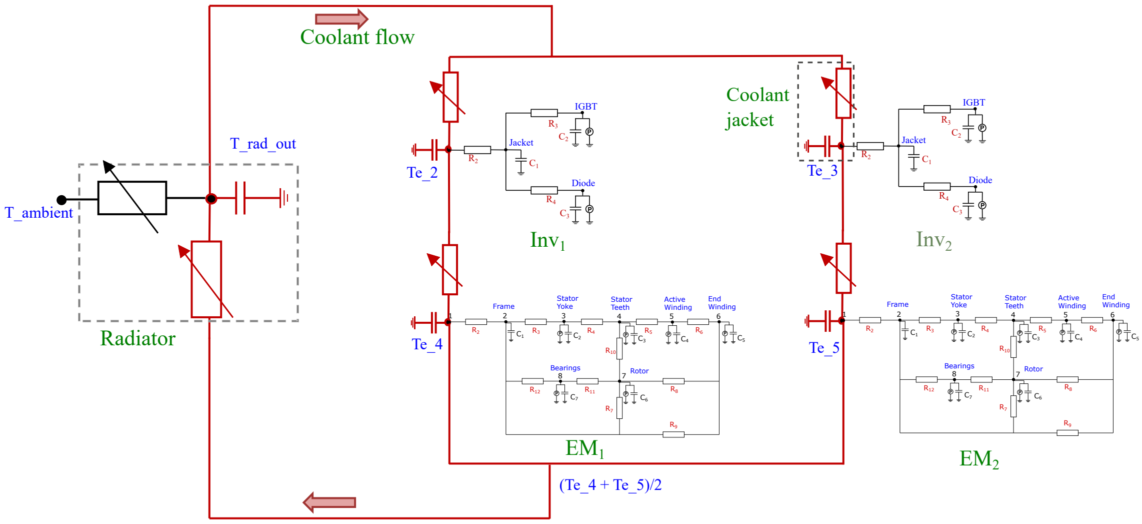

Figure 3.3: Combined thermal model

3.2.2 Coolant circuit model

The coolant circuit model is shown in red lines in the figure 3.3. It is modeled in the form of a lumped parameter fashion having five nodes, one each for the components and one for the radiator. Each node has a thermal capacitance and a resistance. The thermal capacitance is a measure of the thermal mass of the system. The thermal resistance is the inverse of thermal conductance which represents how easily heat can flow between the two connected nodes. Thermal resistance are a function of the mass flow rate of the coolant.They are shown as variable resistances in the figure. A variable thermal resistance connects the $T_{rad,out}$ node to the ambient node, which represents the air side heat transfer of the radiator.

3.2.3 Simplified thermal model

Figure 3.3 shows the complete thermal model with the 25 nodes (1 for radiator, 7 per electric machine, 3 for each inverter and 4 for cooling jackets) and 18 power inputs (7 per EM and 2 per inverter). Out of these, only five critical node temperatures are required for control algorithm, namely, the end winding temperature for both electric machines, inverter IGBT temperatures and coolant temperature at radiator outlet. These critical nodes reach highest temperature at their respective component level and hence, needs to be monitored.
The complete thermal model with 25 nodes is computationally expensive for the controller. A simple thermal model which can estimate the temperature at the five critical nodes is sufficient. The model order reduction method uses a systematic way to reduce the number of nodes to make the model computationally tractable. But it does not reduce the number of inputs to the system. Hence, a lumped model was developed for electric machine and inverter using system identification. The system identification approach considers a 1^{st} order model having a single node representing either the end-winding temperature or the rotor temperature depending upon the R (thermal resistance) and C (heat capacity) values selected.

3.2.3.1 System identification approach

A single node representing the lumped electric machine and inverter components is shown in figure 3.4. The node is connected to the coolant temperature via a thermal resistance. A thermal capacitance represents the thermal mass of the system. The input to the node is the total power loss of the electric machine.Constant coolant flow rate is considered to have constant thermal resistance. The R and C parameters need to be recalculated as the power loss to system is lumped.

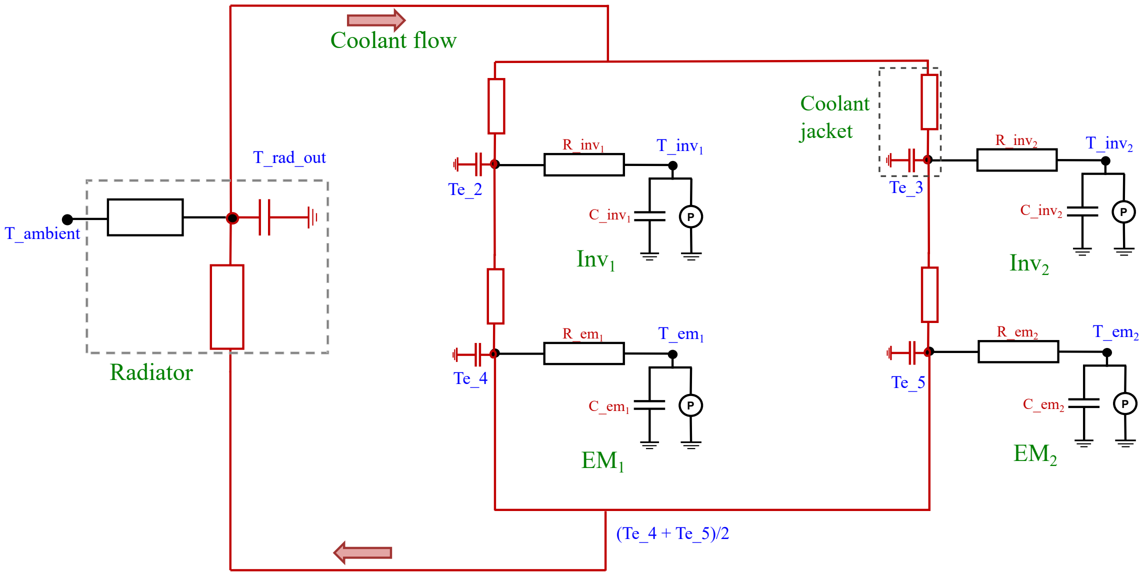

Figure 3.4: Complete thermal model with simplified component models

The R and C parameter identification method is explained in algorithm 1.

Using parameter identification principles, different step inputs of speed and torque are applied to the high fidelity thermal model. This is done at a constant coolant temperature and flow rate. The first step is to obtain the different power losses which are applied on to the different components. The power loss obtained is not exactly following the speed/torque profile but is instead increasing as the time increases and then reaches to a steady value. In the next step using the steady state power loss values as step input, the temperature of the required component is calculated. Figure 3.5 shows this procedure for a speed and torque value of 2000 RPM and 100 Nm. The temperature of end-winding is taken as output in this case.

The temperature is approximated to a first order model as shown in equation 3.3 with combined power loss as an input to the system.

$$T_{k+1} = T_k \cdot (1 - \frac{dt}{RC}) + P_{loss,k} \cdot \frac{dt}{C} + T_{coolant} \cdot \frac{dt}{RC} \tag{3.3}$$

where dt is the frequency at which the temperature calculation is done. R value is calculated as shown in equation 3.2.3.1.

$$R = \frac{Temp_{steadyState} - Temp_{initial}}{Power_{combined,steadyState}}$$

Algorithm 1: Parameter identification for one node component thermal model

Result: Thermal Resistance and Capacitance determination

for *i=1:*N_{temp} **do**
  for *j=1:*N_{rpm} **do**
    for *k=1:*N_{tq} **do**
      STEP 1: Create step input of rpm and torque;
      STEP 2: Calculate power loss;
      STEP 3: Estimate steady state power loss;
      STEP 4: Create step input of power loss using values obtained in STEP 3;
      STEP 5: Calculate temperature rise of End winding/Rotor;
      STEP 6: Estimate steady state value and time;
      STEP 7: Calculate thermal resistance R ;
      STEP 8: Calculate initial thermal capacitance C_{in} *;*
      STEP 9: Set range for C identification using C_{in}*;*
      STEP 10: **while** *C in C range* **do**
        Calculate temperature rise using R and C;
        Quantify deviation from temperature rise curve obtained from simulation using 2^{nd} *order norm;*
      end
      STEP 11: Find C having least deviation;
      STEP 12: Save R and C values;
    end
  end
end

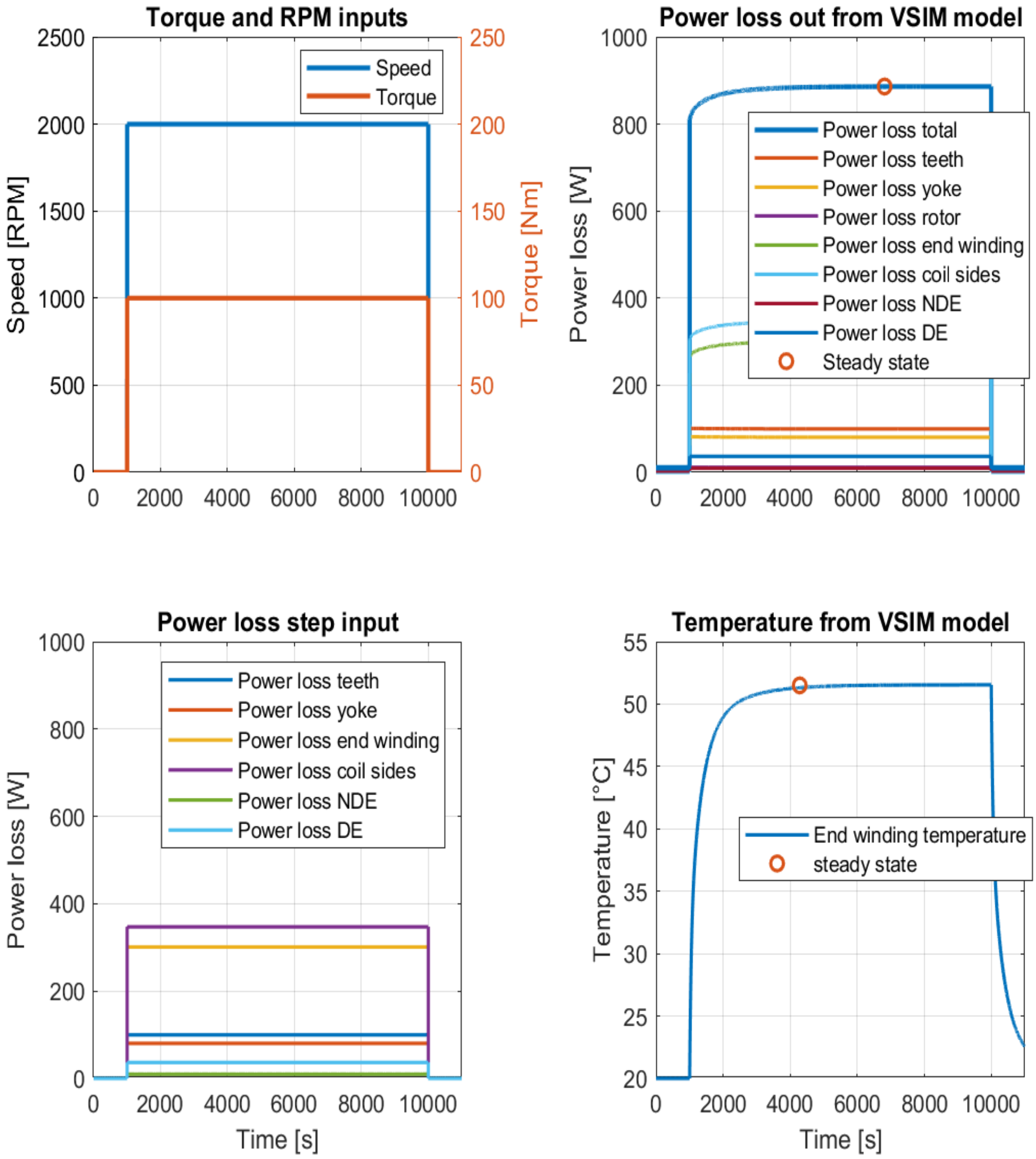

Figure 3.5: Method for performing parameter identification

For the calculation of the C value it was considered that it takes around $5RC$ time for the temperature to reach steady state. This gave an initial estimate of the C value. High deviations in temperature calculation was observed with incorrect C values. So another step was added in which the C value was varied in the range between $0.1 \cdot C_{in}$ to $10 \cdot C_{in}$. Temperature from the first order model was calculated for each C in this range and the 2^{nd} order norm error was calculated with respect to temperature obtained with high fidelity VSIM thermal model. This is shown in figure 3.6. The C value with the least error was selected and considered in further calculations.

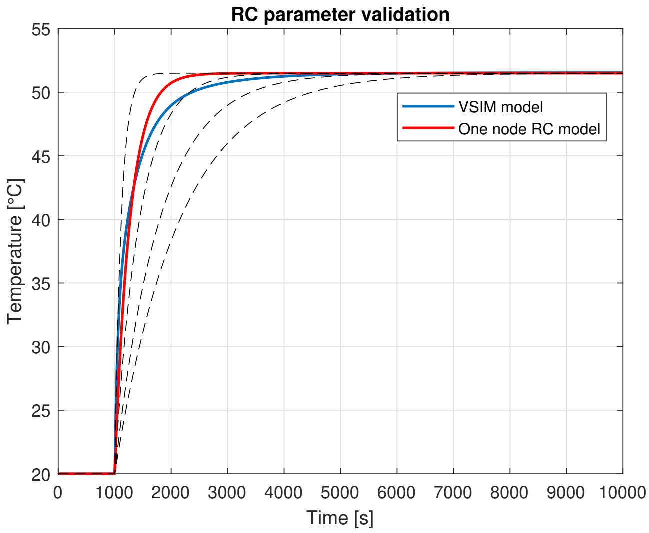

Figure 3.6: Calculation of C to have minimum transient temperature deviation

Different sets of R and C are obtained for end-winding and the rotor temperature. R and C values obtained are dependent on torque, ω , $T_{coolant}$ and mass flow rate of coolant.In this study, the mass flow rate of the coolant is kept constant. Figures 3.7 and 3.8 show the variation of R and C parameter with respect to torque and speed for a particular mass flow rate and temperature of coolant.

A further simplification can be done by taking the mean value of R and C and thus removing the expensive interpolation step in the controller.

The inverter is also considered as a single node element where the single node represents the IGBT temperature. The procedure for identifying the R and C parameters is similar to that of electric machine model.

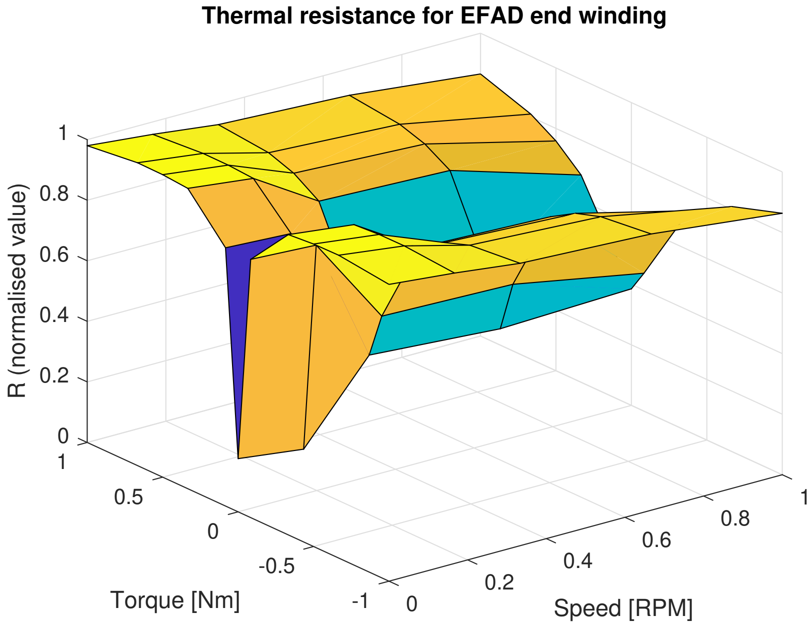

Figure 3.7: End winding thermal resistance variation with torque and Speed

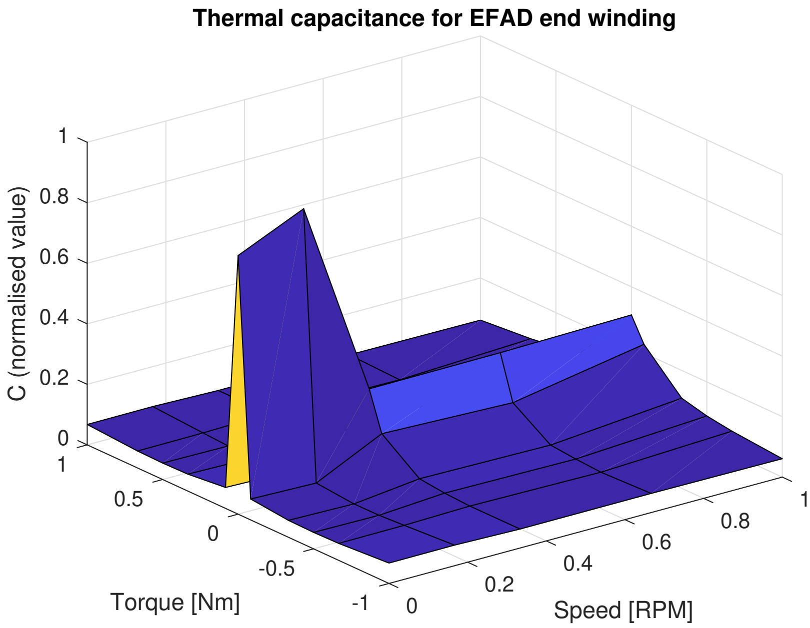

Figure 3.8: End winding thermal capacitance variation with torque and Speed

The simplified thermal model shown in Fig. 3.4 is called the coupled model as the components are linked to each other with the coolant circuit. This model has nine nodes (or temperature states) and four power inputs. The electric machine has reduced to single node and single power input from seven nodes with seven power inputs. Similarly, inverter has reduced from three nodes with two power inputs to single node and single power input. The coupled model was further reduced to only five balanced states with model order reduction and used in online controller.

3.2.3.2 Model order reduction

The state-space system form of the thermal model with lumped components (Fig. 3.4) can be written with the help of transient thermal equation 3.4 as follows:

$$G : \begin{cases} \dot{x} = Ax + Bu, & x(t) \in \mathbb{R}^9, u \in \mathcal{U} \\ y = Cx \end{cases} \tag{3.4}$$

where $X_{9\times1}$ is a vector of 9 nodal temperature, $U_{4\times1}$ is power loss input vector and $Y_{5\times1}$ is vector of output critical temperature nodes.

A balanced realization of the state-space model was computed using the 'balreal' function in MATLAB [17]. The 'balreal' function also computes the Grammians and transformation matrices from the actual to balanced state-space model. Grammians are like weights, showing the relative effect of each balanced state on the output. The balanced states are arranged in descending order of Grammians. Based on the Grammians obtained, only the first 5 balanced states were found to be sufficient to capture the required output critical temperatures. Using the 'modred' function in MATLAB [18], the remaining states from the balanced system were truncated and a reduced state space model in 5 states was obtained:

$$G_r : \begin{cases} \dot{z} = A_r z + B_r U, & z(t) \in \mathbb{R}^5, u \in \mathcal{U} \\ y_r = C_r z + D_r z \end{cases} \tag{3.5}$$

It is important to note that the balanced states in z are fictitious states, i.e. they don't have any physical meaning. The 9 original states in x have to be transformed in fictitious states z by multiplying with a transformation matrix to initialize the reduced system G_r. This makes the reduced model useful for an online controller such as MPC where the original states can be measured to initialize G_r at each time step. But then the reduced model cannot be used in dynamic programming as all the nine original states need to be updated each instant which makes the problem exponentially complex. A further simplified way of modeling the entire system is to consider the coolant inlet temperature of all the components constant. That constant temperature can be tuned to match the component temperatures for the electric machine and the inverter. This model, shown in Fig. 3.9, is called the uncoupled system level model. It has only four temperature states which makes it useful to implement in dynamic programming.

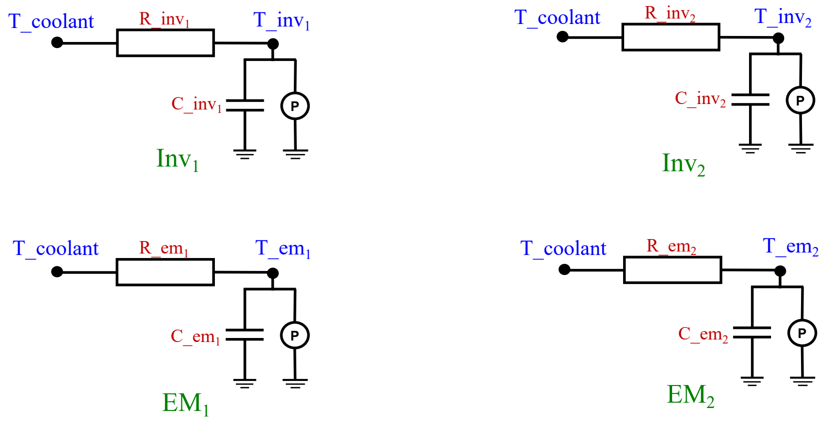

Figure 3.9: Uncoupled system level model with constant coolant temperature for all components

3.2.4 Power loss model for electric machine and inverter

The power loss data of the electric machine is available in a five dimensional interpolation map, where the dimensions are torque, ω, temperature of rotor, temperature of end-winding and the DC voltage. The power loss data of inverter has an additional dimension of the inverter temperature. Accessing power loss data in the form of a lookup table makes it computationally as well as memory intensive for the controller. Hence, a custom equation in torque, rotational speed and temperature was derived to fit the power loss data.

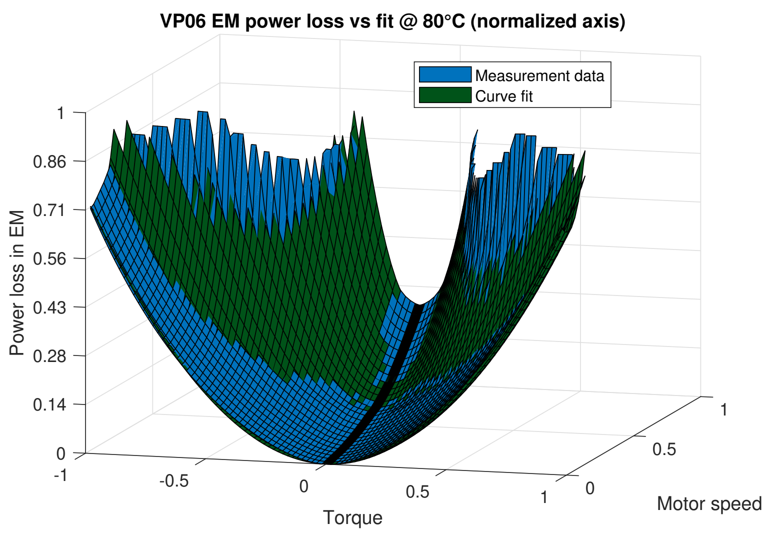

Figure 3.10: Curve fit on electric machine power loss

3.2.4.1 Curve fit power loss model

A custom equation was derived intuitively to fit the power loss map of electric machine and inverter. We observe that the power loss map of electric machine (Fig. 2.7) is parabolic in torque with the curvature becoming sharper as rotor speed increases. This parabola also shifts upwards with increasing speed as magnetic drag loss increase. Hence, the equation should be proportional to square of torque with coefficient proportional to speed. Also, square of speed should be added to capture the upshift. The power loss is predominantly due to copper loss (Fig. 2.6) which increases with temperature due to linear increase in resistivity. Therefore, the effect of temperature was captured in equation by multiplying with a linear factor. The custom equation to model electric machine power loss is as follows:

$$P_{EM} = (1 + \alpha_1 \Delta T)(a\omega^3 + b\omega^2 + c\omega + d)M^2 + (1 - \alpha_2 \Delta T)e\omega^2 \tag{3.6}$$

where,
M = torque,
ω = rotor speed,
ΔT = change in temperature with respect to reference 20°C,
$a, b, c, d, e, \alpha_1, \alpha_2$ = constants.

The value of the constants was obtained by using the curvefit toolbox of MATLAB. Figure 3.10 shows the goodness of fit for the electric machine power loss equation. The fit has an R-square value of 0.98, indicating a good fit.
Similar approach was followed for the inverter. The power loss map of inverter is almost proportional to torque and shifts upwards with increase in speed. Hence, a custom equation to model inverter power loss was devised as follows:

$$P_{inv} = (1 + \alpha_1 \Delta T)a|M| + (1 - \alpha_2 \Delta T)b\omega^2 \tag{3.7}$$

where,
a, b, α_1, α_2 = constants.
Figure 3.11 shows the goodness of fit for the inverter loss equation. An R-square value of 0.97 was obtained for the inverter fit.

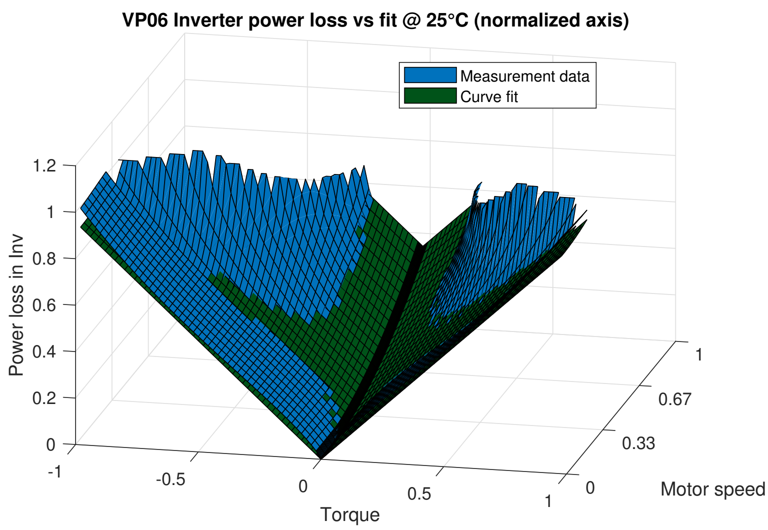

Figure 3.11: Curve fit on inverter power loss

3.2.5 Battery model

The battery is model as just voltage source which changes with state of charge of the battery.

3.3 Optimal control problem formulation

The optimal control problem to determine optimum torque split and clutch control at each time step such that the power losses are minimized can be formulated as follows:

$$
\begin{aligned}
\min_{\lambda_k,\, c_k} \quad & \sum_{k=0}^{N} \Big(P_{loss,EM1}((1-\lambda_k)M, \omega_1, T, U_{DC}) + P_{loss,EM2}(\lambda_k M, c_k\omega_2, T, U_{DC}) \\
& + P_{loss,Inv1}((1-\lambda_k)M, \omega_1, T, U_{DC}) + P_{loss,Inv2}(\lambda_k M, c_k\omega_2, T, U_{DC}) \Big) \\
\text{s.t.} \quad & T_{k+1} = AT_k + Bu_k & k = 0, \dots, N, \\
& T_k < T_{limit} & k = 0, \dots, N, \\
& -M_{EM1,limit} \leq (1-\lambda_k)M \leq M_{EM1,limit} & k = 0, \dots, N, \\
& -M_{EM2,limit} \leq \lambda_k M \leq M_{EM2,limit} & k = 0, \dots, N, \\
& \lambda_k \in [0,1] \qquad \text{/Torque split} & k = 0, \dots, N, \\
& c_k \in \{0,1\} \qquad \text{/Clutch} & k = 0, \dots, N
\end{aligned}
\tag{3.8}
$$

where, λ_k is the continuous torque split variable, c_k is the discrete clutch control variable (0 = disengage, 1 = engage), M is the driver demanded torque and T_k is the critial temperature vector at each time instant:

$$
T_k = \begin{bmatrix} T_{radout} \\ T_{EM1} \\ T_{EM2} \\ T_{Inv1} \\ T_{Inv2} \end{bmatrix} \qquad u_k = \begin{bmatrix} hT_{ambient} \\ P_{loss,EM1} \\ P_{loss,EM2} \\ P_{loss,Inv1} \\ P_{loss,Inv2} \end{bmatrix}
$$

The condition on λ_k is such that:

$$
\begin{aligned}
\text{if} \quad & c_k = 0 \Rightarrow \lambda_k = 0 \\
\text{else} \quad & c_k = 1 \Rightarrow \lambda_k \in [0,1]
\end{aligned}
$$

3.3.0.1 Considerations while formulating the objective function

The objective function was formulated as the sum of the power loss of four components-front and rear inverters and electric machines. The pump power loss was omitted from the objective function as constant coolant flow rate was considered. The decision to ignore pump losses and to have constant coolant flow rate was based on the fact that even at full speed, the total pump losses were not significant in comparison to losses from other components.Adding pump losses therefore will add complexity to the problem with no significant changes to the result obtained.

The clutch engagement and disengagement is also not penalised. During disengagement in actual operation the torque of the electric machine is modulated to ensure that speed of the rotor becomes zero as fast as possible with a separate PID controller in the inverter. This means that every clutch disengagement action is associated with a certain energy benefit. The reverse is true for clutch engagement which has a positive energy requirement.This extra energy is a function of speed difference during clutch actuation. This energy has been ignored in the current formulation. Although, the plant has been modeled to have different torque considerations during clutch engagement and disengagement phase.

3.4 Controller

3.4.1 Dynamic Programming

As explained in the section 2.5.1, dynamic programming can be used to provide a benchmark optimal solution. The pseudo-code used for DP implementation is shown in algorithm 2. The objective function of the optimal control problem was minimised for the entire drive cycle. Constraints are implemented in the form of penalty functions and added to the objective function. As dynamic programming computational time is dependent on the number of states and its discretization, the uncoupled 4 node thermal model is used. This reduced the 5 states of the coolant circuit. For electrical machine the power loss depends on both end winding and rotor temperature and thus both these states are considered. For inverter, IGBT temperature is considered. Component thermal limits is imposed on end winding and IGBT temperature.

For selecting the number of discretization a study was done in which the effect of discretization was quantified. For this study, DP with just 2 states- end winding temperature of front and rear machine was considered. This was done as with two states we can increase the number of discretization without getting constrained by the memory or time limit. Five cases were taken with temperature discretization of 5,10,15,20 and 30$°C$. In all these cases the energy loss was calculated for high speed highway driving cycle. There was no significant difference observed with energy loss in all these cases. This is stipulated to be because of small difference in temperature dependent power losses in the operating zone.These small differences does not add up to make a significant change in energy loss calculation for the complete cycle. Effect was observed when changing discretization near the penalty limit. Thus in all the cases the grid near the penalty limit was kept same.

Table 3.2 shows the different states and their discretization used for DP.

Table 3.2: States and discretization for DP

State name	No of discretization	Type of discretization
End winding EFAD	5	Non uniform
End winding ERAD	5	Non uniform
Rotor EFAD	4	Uniform
Rotor ERAD	4	Uniform
IGBT front inverter	4	Uniform
IGBT rear inverter	4	Uniform
DC voltage	3	Uniform

Algorithm 2: Dynamic programming (set implementation)

Result: Optimal control Policy
for *k=N-1 to 1* **do**
    $G = f(x_{grid}, u_{grid})$;
    $x_{k+1} = f(x_{grid}, u_{grid})$;
    $J_k = G + J_{k+1}(f(x_{k+1}, u_{k+1}))$;
    $J(i_x, k) = minJ_k$;
    $u(i_x, k) = argminJ_k$;
end

Power loss for electric machine is implemented in the form of 5D look up tables. Inverter power loss is implememted in the form of 6D look up table. As DP calculation of optimal policy is done offline having computational expensive interpolation maps is not problematic. The control is discretized in 21 steps.

3.4.2 Model predictive online controller

The control policy obtained from dynamic programming cannot be used in real driving since it is tuned for a particular drive cycle. For a general driving scenario, an online controller is required which calculates the optimal torque split and clutch control instantaneously. An online controller was developed based on model predictive control and tested in simulation environment. The plant model is present in Simulink, hence a ‘Matlab system’ block was used in Simulink to implement the controller. CasADi [19], an open source nonlinear optimization tool, was used to develop the online controller.

Algorithm 3: Model predictive control

Result: Optimal torque split
$t_{horizon}$ = N s;
number of steps = N;
symbolic $\lambda_k \quad \forall k = 0 \ldots N-1$ (control sparse matrix);
symbolic $x_k \quad \forall k = 0 \ldots N$ (states sparse matrix);
parameter $\omega_k, M_k \quad \forall k = 0 \ldots N-1$ (speed, torque prediction);
symbolic cost $= \sum_{k=0}^{N-1} P_{loss}(\lambda_k M_k, \omega_k, x_k)$;
equality constraints $g: \quad x_{k+1} = Ax_k + Bu_k \forall k = 0 \ldots N-1$;
inequality constraints $w: \begin{Bmatrix} x_k < T_{limit} \quad \forall k = 1 \ldots N, \\ 0 \leq \lambda_k \leq 1, \quad \forall k = 0 \ldots N-1, \\ -M_{limit} \leq \lambda_k M_k \leq M_{limit}, \quad \forall k = 0 \ldots N-1 \end{Bmatrix}$;
solver = nlpsol('bonmin/ipopt', cost, variables: (x_k, λ_k), constraint: (g, w));
for *every t = 1s* **do**
    update x_0;
    update ω_k, M_k;
    solve solver(x_0, ω_k, M_k);
    pass λ_0 to plant;
end

The above algorithm explains the model predictive online controller implementation. First, a mixed-integer 'bonmin' solver [20] was used to take care of the binary clutch variable. But this solver was not able to converge for higher horizon and not reliable near limits. Another option is 'ipopt' solver [21] which is not made for discrete variables. Hence, the effect of clutch was implicitly added to the problem as a logical condition $\omega_2 \cdot (\lambda \neq 0)$ depending on the torque split (λ). This implies if the torque split is zero i.e. all torque is provided by rear axle, the clutch should be disengaged i.e. $\omega_2 = 0$ to prevent magnetic drag losses. Upon implementation, the 'ipopt' solver was missing the global optimum at $\lambda = 0$ and converging at local optimum with non-zero torque split for some parts of the drive cycle as shown in Fig. 3.12. Hence, a hybrid heuristic+MPC controller was developed which would calculate cost considering constant zero split over horizon and compare with the MPC solution. If the cost of zero split is lower then that would be applied instead of MPC solution. The power loss maps were included in the form of custom curve fit equation as explained in section 3.2.4, instead of lookup tables. This reduced the computation time by a factor of 3.

The sampling period and horizon are important characteristics of an MPC controller which affects its performance. In this case, the sampling period determines how frequently the torque split and clutch control will be updated. Since, this affects the vehicle handling, a quick response in torque split is expected. If the driver presses throttle hard to demand high torque the torque should be split uniformly and clutch should be engaged so that a single motor doesn't saturate on limit. A sampling period of 1 second was selected considering it to be enough to match the driver response.

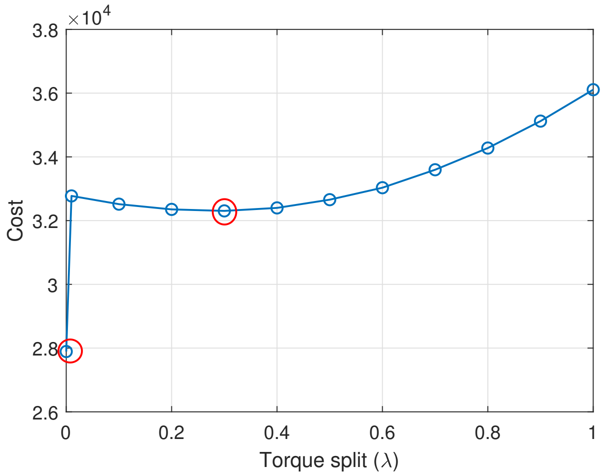

Figure 3.12: Cost for different torque split for some snap of drive cycle

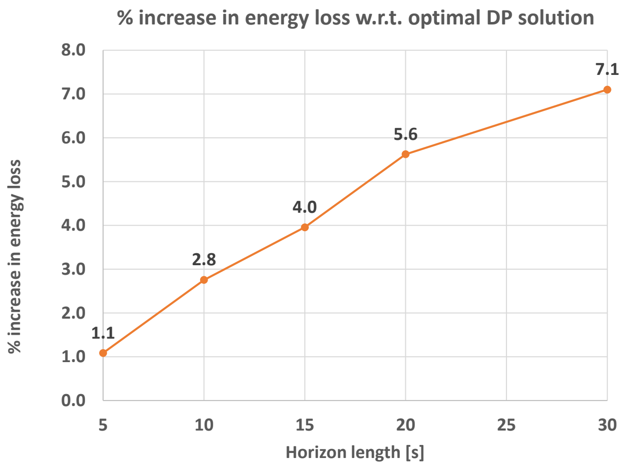

Figure 3.13: Effect of horizon on energy consumption

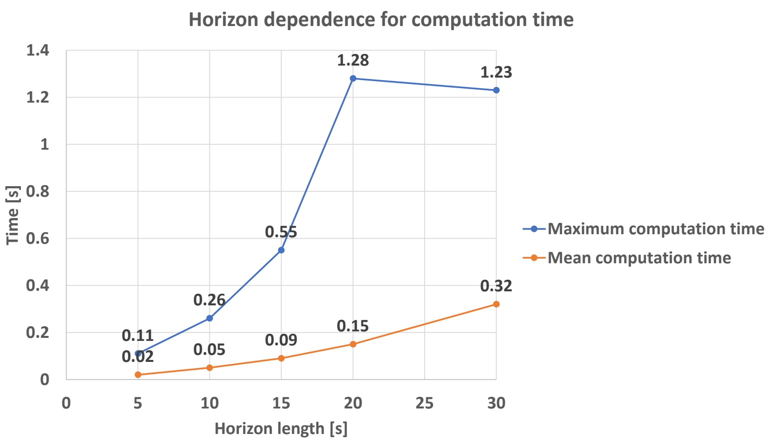

Figure 3.14: Effect of horizon on computation time

The thermal response is slower than the vehicle dynamic response. Hence, to capture the effect of prediction on temperature, a larger horizon is desirable. But since the sampling time is fixed at 1 second, a larger horizon will increase the number of equations in the optimal control problem which affects the computation time. A study was conducted to determine a suitable horizon. Fig. 3.13 and 3.14 shows the effect of horizon on energy consumption and computation time respectively for a typical city drive cycle. We see that the mean as well as maximum computation time increases with horizon as expected, since the number of equations increase at the fixed time step. The energy loss showed an increasing trend with higher horizon as the controller becomes more conservative. This can be observed towards end in Fig. 3.15. The controller with horizon 30s is being more conservative when the temperature of end winding reaches near limit as compared to controller with horizon 5s. Seeing these two effects, a horizon of 5s was selected.

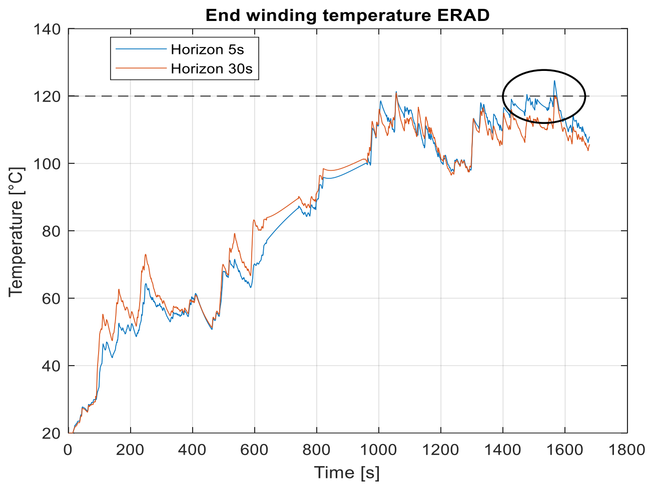

Figure 3.15: Effect of horizon on end winding temperature limit

3.4.3 Static+heuristic controller

The static controller developed in the previous study was also modified with added heuristic rules to prevent the temperature of critical components exceeding safe limits. The temperature zone was divided into three range. Below the first limit the torque split is governed by the static controller. As the temperature reaches the first limit, a constant torque split of 0.5 is imposed. This is changed to 0.8 when temperature reaches the second limit and 1 when temperature reaches the third limit. If temperature of front motor also reaches the third limit then both the motors are operated at 0.5 torque split. Figure 3.16 details the heuristic rule applied on top of the static controller.

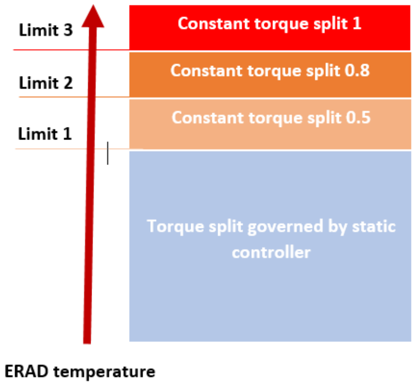

Figure 3.16: Heuristic rule added on top of static controller

3.5 Temperature dependent power loss maps

In static controller, the power loss maps are calculated for a nominal temperature. The controller decides the split according to power loss at this temperature. In the powertrain configuration selected, the front and rear motor have different power loss characteristics. This along with dynamic splitting of torque and clutch actuation can lead to motors operating at different temperatures. Including temperature dependent power loss data in the controller will ensure that controller selects a more efficient torque split. Increased difference in temperature between the two machines is observed in drive cycles having operating points with high power loss and torque demand such that it can be fulfilled by a single machine.
Figure 3.17(a) plots the contours for difference in power loss when the clutch is disengaged and when the clutch is engaged for different operating region as per equation:

$$\Delta z = P_{loss,\lambda=0,c=\text{disengaged}}(M, v) - P_{loss,\lambda=0.4,c=\text{engaged}}(M, v) \tag{3.9}$$

The x-axis depicts the vehicle speed and the y-axis shows the wheel torque. Only the region that can be met with a single machine is shown. Above this region the torque requirements necessitates the use of both the machines. The machines are at room temperature which in this case is 20°C. During clutch engagement, a constant torque split of 0.4 is considered. This is done for reference purpose and it does not exactly replicate the behaviour of the dynamic controller. The red line shows the boundary below which it is beneficial to run the vehicle in the clutch disengaged condition. In this area the magnetic drag losses overcome the increased power loss associated with rear machine operating at high torque regions. This is important as the power loss is proportional to square of the torque and increases quadratically as torque increases. For a driving cycle, if the operating points fall continuously below this line, the clutch remains disengaged and the rear motor gets heated up. Based on the overall duration the points stay below this line, the machines built up a temperature difference. The power loss changes with the temperature of the machines and so does the line below which disengaging clutch is beneficial. Figure 3.17(b) shows an

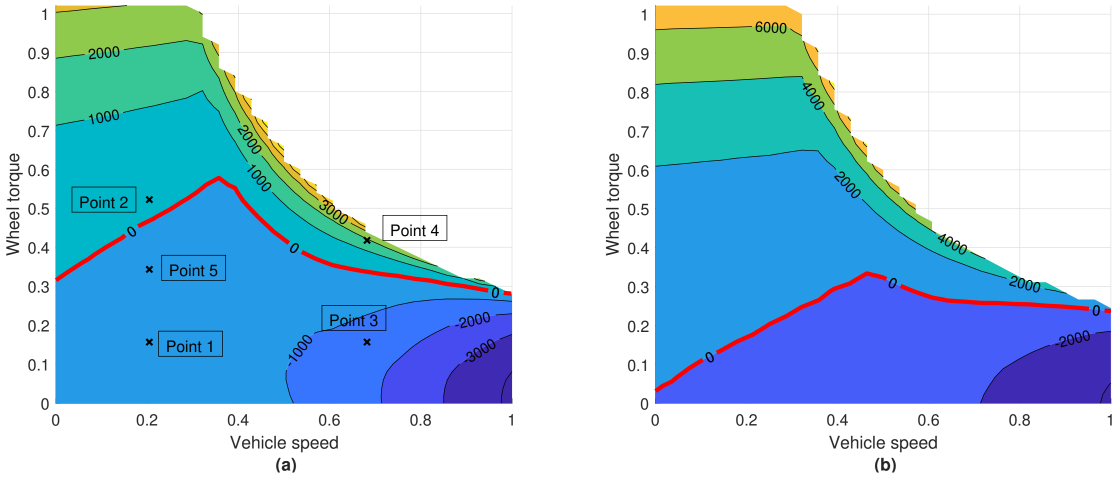

Figure 3.17: Difference in power loss for clutch disengaged and clutch engaged case with front motor at 20°C and rear motor at (a) 20°C and (b) 150°C

extreme case, where rear machine is at 150°C and the front machine is at 20°C. In this case, the zone where clutch disengagement is beneficial has reduced. This clearly indicates that including temperature dependent power loss maps will change the optimal torque split. The magnitude of change will depend upon the drive cycle and the temperature difference it will create.
In order to quantify the benefit of adding temperature dependent power loss maps, the controller was tested at some constant operating points. Constant operating points were selected as it becomes easy to analyze the controller behaviour in these conditions.These points represents the different zones in the power loss maps as shown in 3.17(a). The vehicle is operated at these operating point for a certain time duration. The duration was selected to ensure that the temperature limit is not reached. In every case, the vehicle is soaked to an initial temperature of $20°C$. Table 3.3 shows the operating points and the duration for each test case.

Table 3.3: Test cases for analysing the effect of including temperature dependent power loss maps

	Zone	**Wheel Torque [Nm]**	**Motor Speed [RPM]**	**Duration [s]**
Point 1	Low Torque/Low Speed	701	2865	600
Point 2	High Torque/Low Speed	2192	2865	600
Point 3	Low Torque/High Speed	701	9549	600
Point 4	High Torque/High Speed	2192	9549	250
Point 5	Medium Torque/Low Speed	1535	2865	1000

Two cases were considered-

1. Case 1: Power loss maps with constant temperature (70°C)
2. Case 2: Power loss maps dependent on temperature.

Dynamic torque split was achieved by running DP controller.In case 1 with power loss at constant temperature, the controller action was similar to static controller. The energy loss with both the cases were recorded and compared to find the effect of temperature dependent power loss maps.Since the operating points are within the limits the torque split is governed by power losses only. Any change in torque for the two cases will be a result of different power loss based on temperature. The difference in energy for the different operating points are given in the results section.

4

Results

4.1 Validation of simplified thermal models

4.1.1 Validation of single node R and C values

The R and C values obtained in section 3.2.3.1 were verified by comparing the temperature obtained by the high-fidelity base model against the one-node simplified model. The coolant flow rate and temperature was maintained constant for the entire drive cycle. Comparisons are made for the end-winding and rotor temperature of the electric machine and the IGBT temperature of the inverter. The lumped R-C values are a function of torque, ω and the temperature of the coolant. Figure 4.1 shows the behaviour of the single node model against base model for WLTC drive cycle by considering $R - C$ in both matrix form (R/C = f(Tq,ω,$T_{coolant}$) and as a mean value.

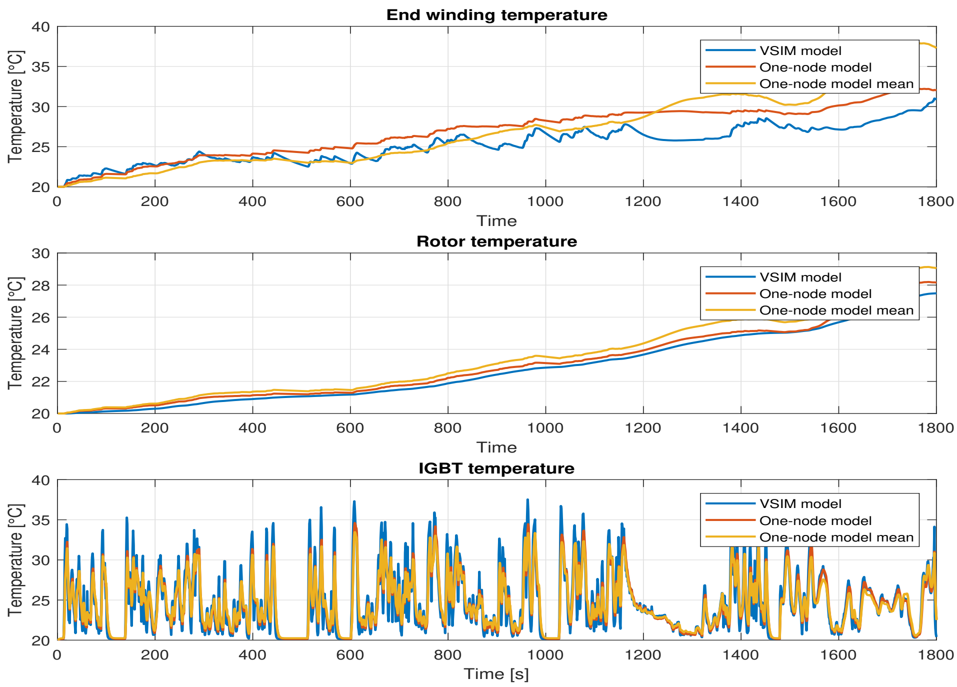

Figure 4.1: Comparison of one node RC model

In order to quantify the temperature variation and to understand the significance of the this temperature delta, the square of temperature difference at each time instant were divided by square of the absolute temperature given by the high fidelity model.Taking the square root of this value gives the relative temperature difference at that time instant. Mean of the relative temperature difference was calculated for the entire drive cycle. This normalised this error value with respect to cycle length. Finally the error percentage was calculated and compared for different drive cycles. Equation 4.1 shows the formula used for calculating this error percentage.

$$Error\% = mean\left(\sqrt{\left[\frac{Te_{GT}-Te_{simple}}{Te_{GT}}\right]^2}\right) * 100 \tag{4.1}$$

Table 4.1 shows the error percentage value for two drive cycles.

Table 4.1: Mean error percentage in temperature calculation using single node R and C values

	WLTC		**City drive cycle**	
	RC matrix	RC mean	RC matrix	RC mean
End-winding	6.5	8.1	15	14
Rotor	1.2	2.9	3	2.2
IGBT	4	4.3	8.4	8.8

4.1.2 System identification approach

The performance of the reduced model with system identification approach for the city drive cycle is shown in figure 4.2. There is a good match to all the different temperatures except slight over-prediction in some cases.

Table 4.2: Mean relative temperature difference percentage for reduced model using system identification approach

	Artemis Highway	WLTC
Front motor end winding	11	1
Rear motor end winding	6	3.5
Front motor rotor	4	2
Rear motor rotor	5	1
Front inverter IGBT	14	5
Rear inverter IGBT	6	6

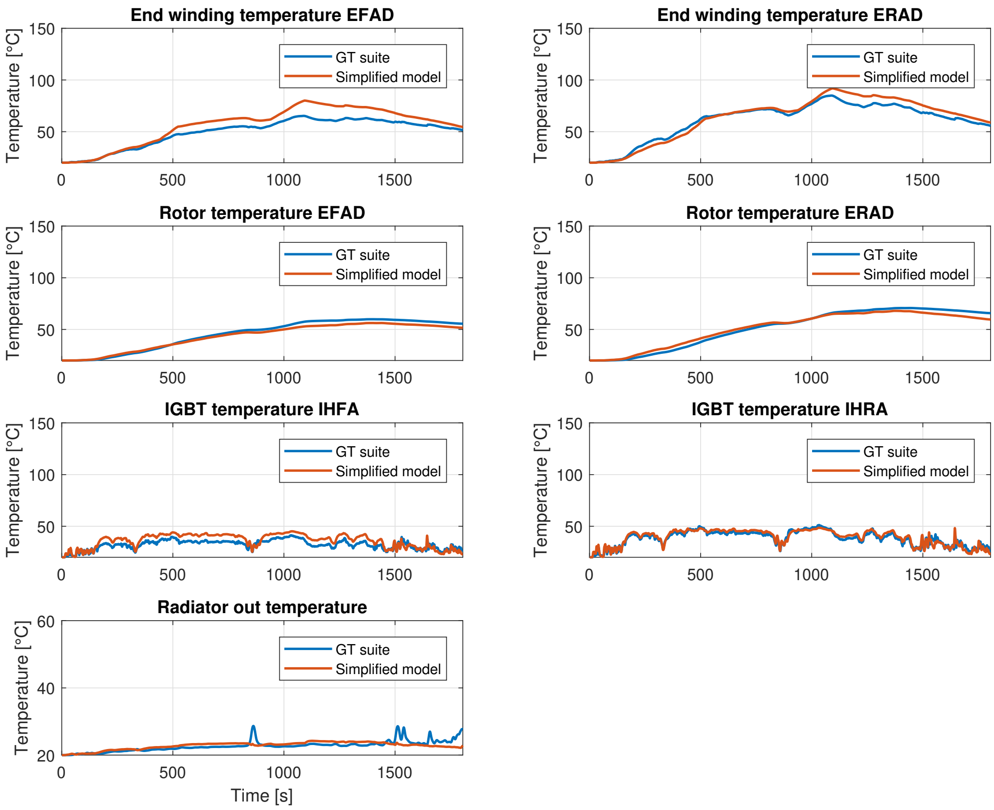

Figure 4.2: Verification of thermal model reduced using system identification approach

An important consideration here is to ensure that this model gives acceptable performance under different driving conditions. Table 4.2 shows the error percentage value for two different drive cycles. The maximum error percentage obtained was around 15%. Considering that this is a very simplified model, and this model is to be used in the controller, this much error was considered acceptable.

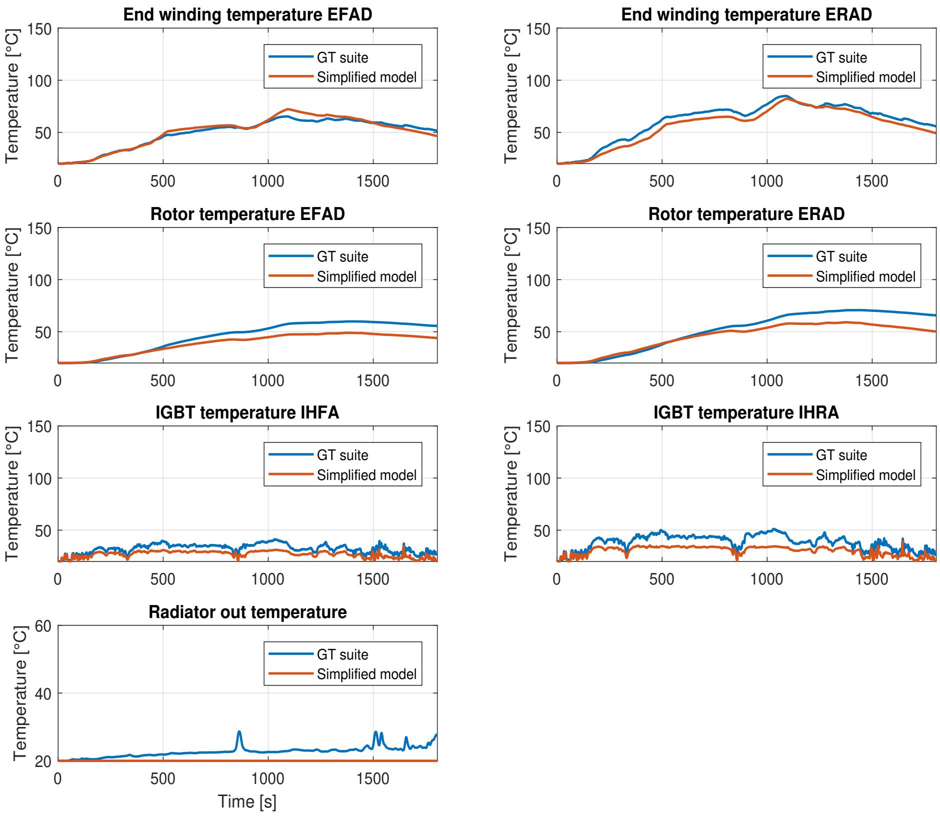

Figure 4.3: Verification of 4 state thermal model used in DP

For dynamic programming, this model was further simplified as explained in the last part of section 3.2.3. The results of such a modification is shown in figure 4.3. The end-winding temperature have a good match, but there is a drift in rotor temperature. This is because of constant radiator out temperature used in the model. As time passes, the temperature of the coolant at radiator outlet increases and this increases the temperature of the components. This is a source of error in DP which is accepted as DP will do a temperature prediction at every 1 second. The benefit with this model was that we could use both rotor and end winding temperature for electric machine power loss calculation. With coupled model because of extra 5 states of coolant circuit this could not have been possible due to computational limitations.

4.1.3 Model order reduction approach

The complete thermal model as shown in figure 3.3 was reduced by applying model order reduction principle. The states are reduced from 25 to 5 (Endwinding temperature of front and rear machine, IGBT temperature of front and rear inverters and radiator outlet temperature). Figure 4.4 shows the comparison of temperature of different components obtained using VSIM thermal model, Reduced model from MOR and the GT-suite model. The reduced model is able to accurately predict the temperature rise. End winding and radiator out temperature has more fluctuations compared to GT-suite predicted temperature. This can be attributed to the selection of states which includes IGBT temperature which has high fluctuations. During mathematical reduction thermal behaviour of IGBT temperature has influenced the end-winding and radiator temperature determination.

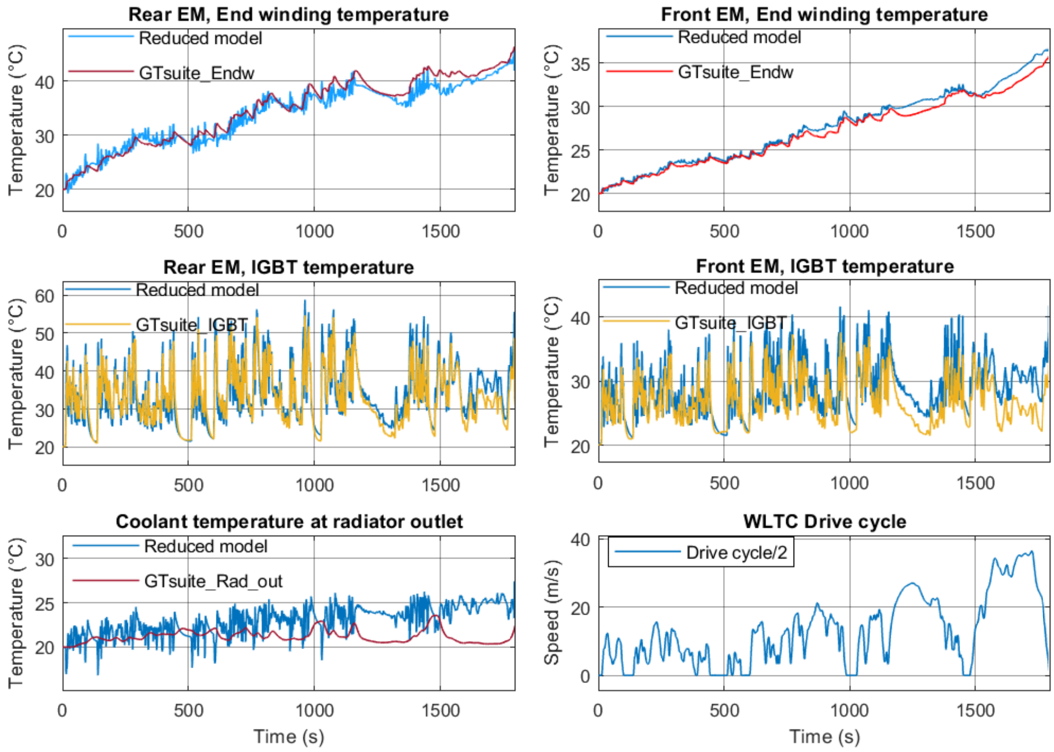

Figure 4.4: Verification of thermal model reduced using model order reduction

4.2 Temperature monitoring using dynamic controllers

The static controller developed in the previous study was implemented for Volvo's power-train configuration. This controller takes no account of thermal dynamics and there is a chance that the components can exceed their thermal limits. For visualising this condition, a high-speed highway drive cycle was created in which the vehicle is driven is at a constant speed of 52 m/s. This is a very high speed and is not exactly representative of highway driving conditions. This drive cycle was chosen as it enabled the components to reach their thermal limit in a relatively short span of time. In this case, the electric motors was able to reach their end-winding temperature limit in just 1 hour. A more realistic cycle with highway speed around 33-44 m/s will not be able to reach the thermal limit within feasible simulation time range. Since, the purpose of this drive cycle is to evaluate the performance of the controllers at extreme thermal conditions, its use here can be justified. This cycle is an energy intensive cycle and utilises the complete battery of the vehicle. Thus torque limit variation with DC voltage is also captured in this cycle.

Figure 4.5 shows the result for dynamic torque split using static controller. The front electric machine is called EFAD (Electric front axle drive) and the rear electric machine is called ERAD (Electric rear axle drive) in these images. The drive cycle torque and speed requirements are such that running a single machine is the ideal torque split strategy here. The rear machine is continuously operated and gets heated up quickly. It can be seen that at near 3000 seconds the temperature of end-winding of rear machine has exceeded the limit. IGBT temperature is well within the limits in this case.

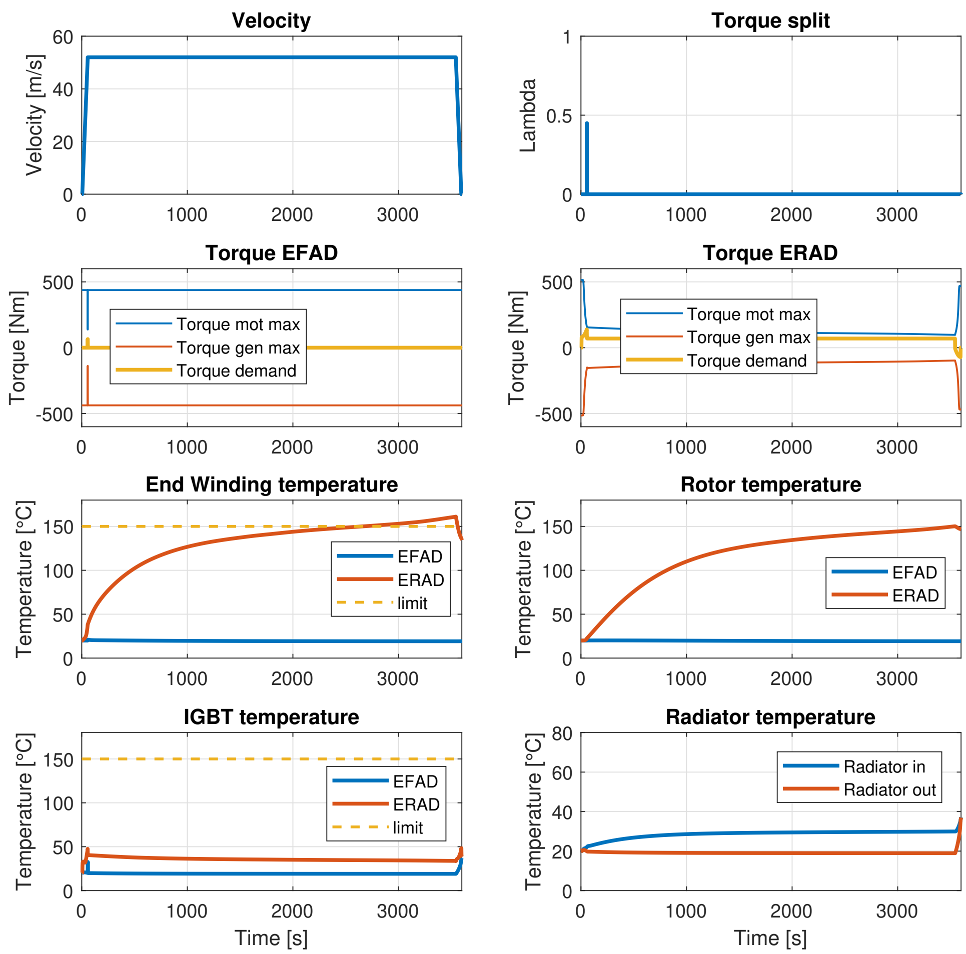

Figure 4.5: Static controller performance for high speed highway cycle

For the same driving cycle,the performance obtained by the static+heuristic controller is shown in figure 4.6. Adding heuristic rule to static controller has the advantage that it can restrain the temperature to within the limits. But, the heuristic rules are not optimal and will be on a conservative side. This effect is seen clearly in the rear electric machine end winding temperature. As soon as the end winding temperature reached the first limit at around 1350 seconds, the controller changed the torque split from 0 to 0.5. With 0.5 torque split the power loss of the rear machine reduced and this led to lowering of the temperature of end winding.The controller switches the torque split to 0 to minimise the total power loss. With rear machine again delivering the complete torque its power loss and temperature increases. The controller thus fluctuates the split between 0 and 0.5 to maintain the temperature. Figure 4.7 shows this effect in detail.

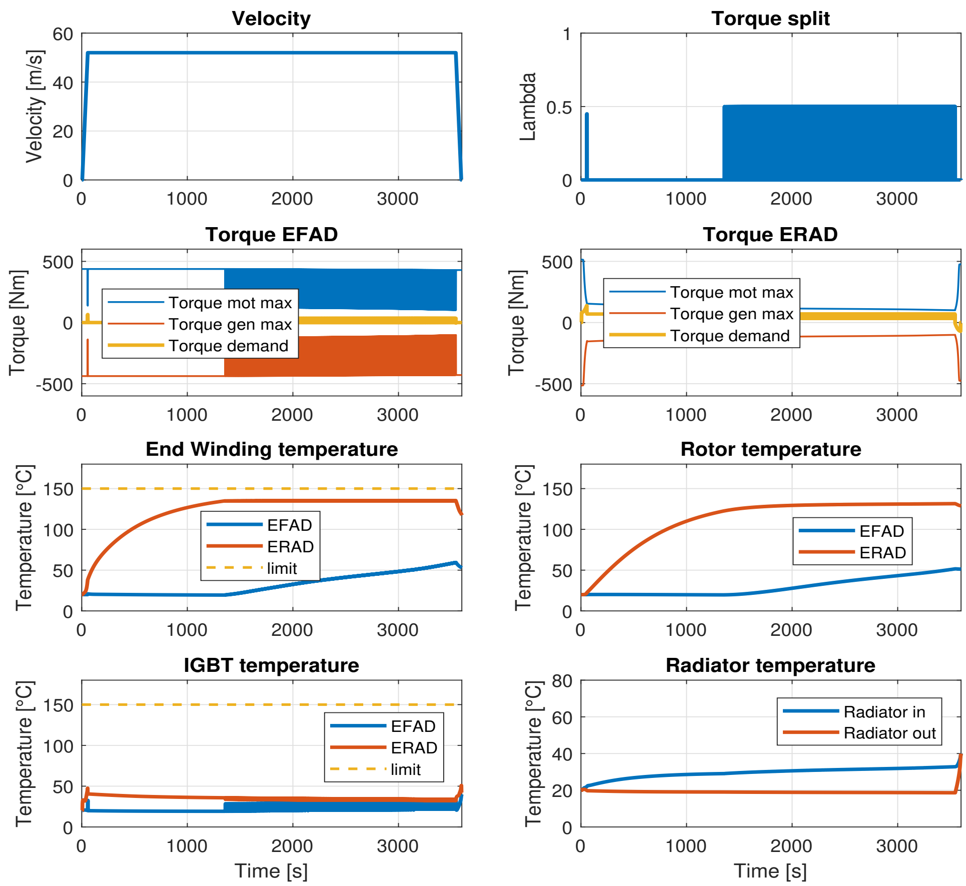

Figure 4.6: Static+heuristic controller performance for high speed highway cycle

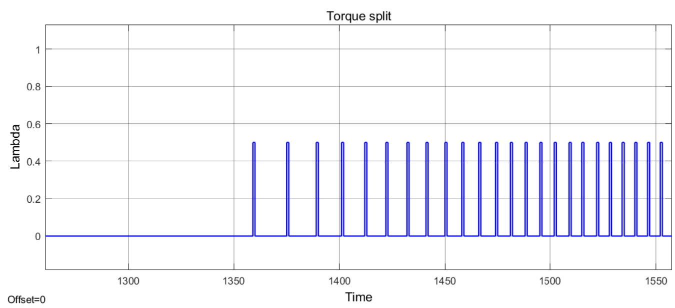

Figure 4.7: Enlarged view of torque split at time period when end-winding temperature approaches the limit

The end winding temperature of front machine shown by EFAD in the figure starts increasing at around that time because of its increased engagement in delivering the torque. The fluctuations in the maximum/minimum torque of front machine is because of the limit change due to speed of the machine which changes between 0 and the operating rotor speed.

Figure 4.8 shows the performance for the DP controller. As DP has complete information of the drive cycle it is able to maximise the benefit by delaying engagement of front machine to around 2700 seconds. The controller changes the torque split from 0 to 1 as this configuration has the lowest power loss. This is different than the control action selected by static+heuristic controller.Static+heuristic controller has information of just the present condition and it applies gradual step wise torque split strategy with regards to temperature limit to ensure that component limits are never exceeded.

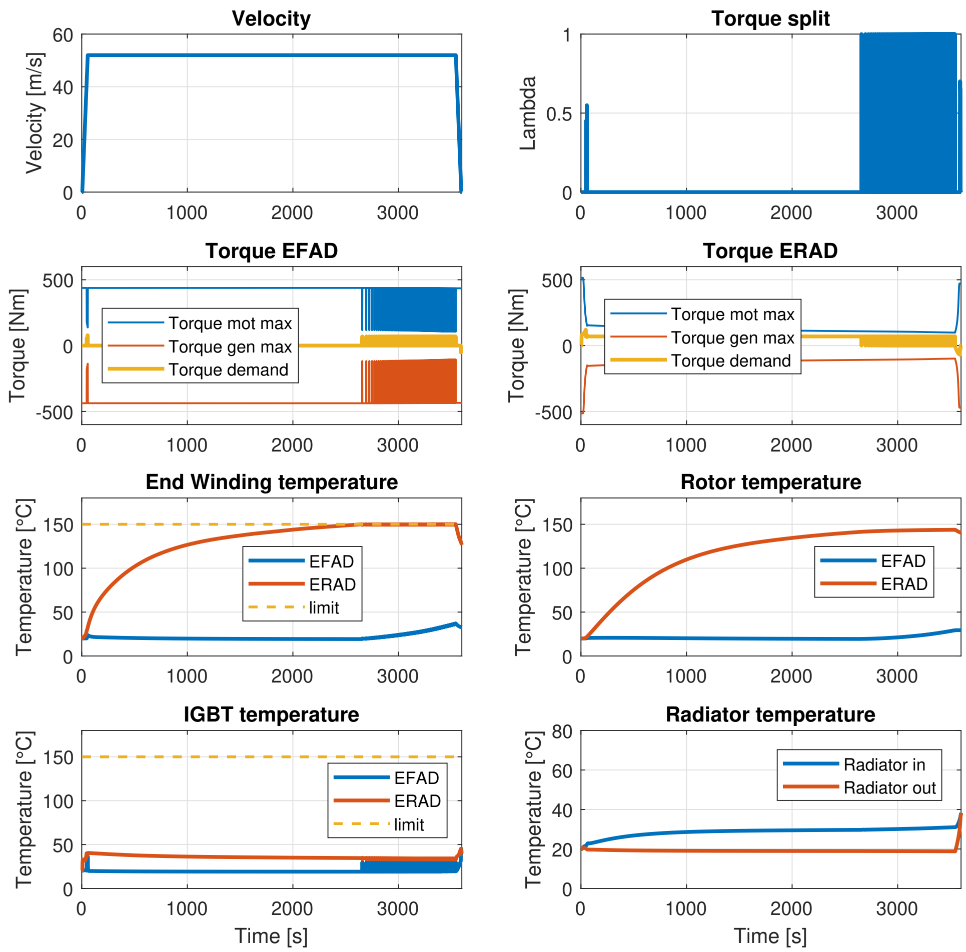

Figure 4.8: DP performance for high speed highway cycle

Figure 4.9 shows the performance of MPC controller. It is also able to restrict the temperature within limits and has a performance very similar to DP.

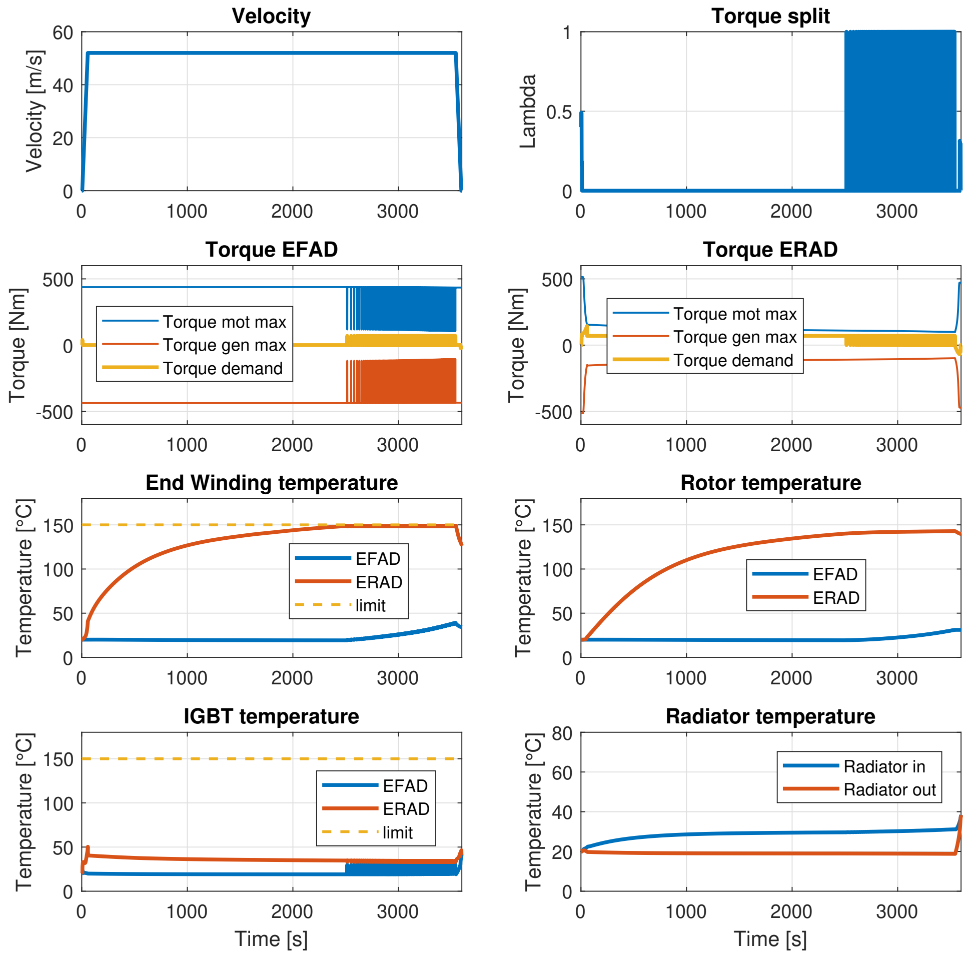

Figure 4.9: MPC controller performance for high speed highway cycle

4.3 Effect of temperature dependent power loss maps

Figure 3.17(a) shows the five points plotted on top of the power loss map. Points 1,3 and 5 fall in the clutch disengaged zone at low temperature. Points 2 and 4 lie outside this zone and will have both the machines engaged from the start.

Table 4.3: Difference in energy loss when we consider temperature dependent power loss maps

	Case 1-Static		**Case 2-Dynamic**		
	ΔT_{endw}	Energy loss[kWh]	ΔT_{endw}	Energy loss[kWh]	% Energy difference
Point 1	18	0.2674	18	0.2674	0
Point 2	26	0.8602	20	0.858	0.26
Point 3	60	0.69	60	0.69	0
Point 4	35	0.8632	24	0.859	0.49
Point 5	73	1.016	50	1.012	0.39

Table 4.3 shows the temperature difference and energy loss for the five points for both the cases. Case 1 is for static controller where power loss is calculated at constant temperature. Case 2 is for dynamic controller where electric machine and inverter power loss are a function of temperature.

For Point 1 and 3, there is no change in energy loss when we compare the two cases. This is because these operating points fall under the line below which clutch disengagement is the optimal policy. As the clutch remains disengaged in both the cases, the energy loss is same. The end-winding temperature difference between rear and front machine has no effect for these points.

For points 2 and 4, since there is an engagement of both the machines, the temperature difference generated for the entire drive cycle between the machines is small. A slight reduction in energy loss is observed in these cases.

Point 5 has a single motor running in the beginning but as time proceeds the temperature dependent loss becomes significant and the clutch gets engaged.This case also shows a positive benefit in the energy loss.

The benefit obtained by including temperature dependent power loss maps was found to be limited to certain zones only. For the cases tested, the benefit observed was not much and it was concluded that for the selected powertrain configuration, the effect of including temperature dependent power loss maps has no significant improvement. This is further tested with continuous drive cycles and the results are shown in section 4.4. In both the city and the combined highway and city drive cycle, where the temperature of the components are within limits, we see that the energy losses obtained by static+heuristic and the DP controller is the same.

4.4 Comparison between different controllers

This section compares the three controllers in terms of energy loss.The torque split provided by these controllers are use to distribute the requested torque between the front and rear machines. The high fidelity VSIM based backward plant model is used to calculate the energy losses in all the three cases. Backward model is used to keep the torque profile same for all the three cases.

In order to capture the benefit of dynamic clutch engagement, these three controllers are compared against a constant torque split of 0.4. This was based on a study done to find the optimal constant torque split without clutch disengagement for the given powertrain configuration.The energy loss for different constant torque split were calculated for four drive cycles as shown in figure 4.10. The torque split with least power loss is selected as the optimal for that drive cycle. The optimal value was found to be between 0.2 to 0.4. With low torque split value, the vehicle will not be able to meet the vehicle torque requirements for high load conditions. Thus the value of 0.4 was selected as the optimum torque split with constant clutch engagement and this was taken as a reference to compare against different controllers.

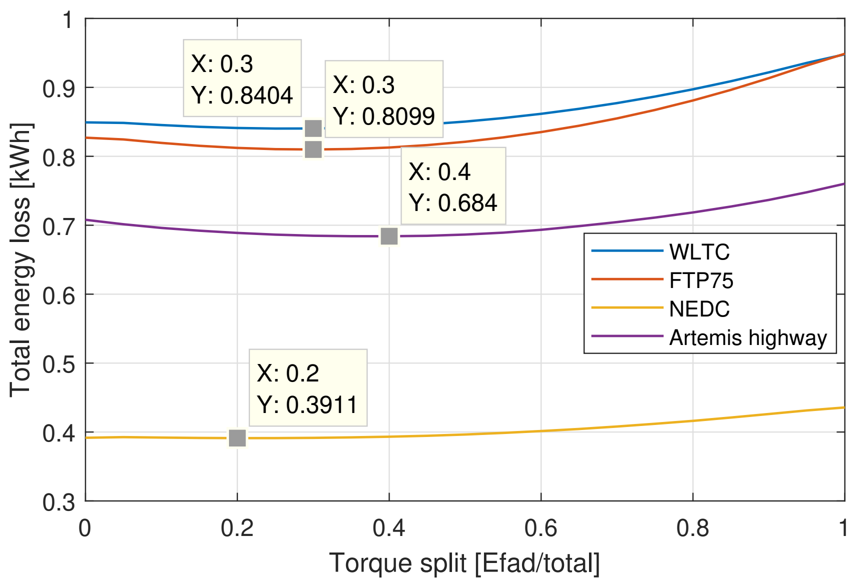

Figure 4.10: Optimal torque split without clutch disengagement

Figure 4.11 shows the total energy loss for the high speed highway cycle for the three controllers when compared against the constant torque split. In all the three controllers, an energy benefit was observed. DP and MPC controller showed the maximum benefit at around 28%. The benefit is because of the savings obtained by removing the magnetic drag losses of the front machine. The difference between static+heuristic and the other dynamic controllers is because of the heuristic rules which are more on a conservative side. The static+heuristic controller does not have future information and thus has a three step control changing torque split to limit the temperature as explained in section 3.4.3. As soon as the temperature reached first zone, the torque split changed to 0.5. Although 0.5 lambda limited the temperature, being sub-optimal it increased the energy loss.

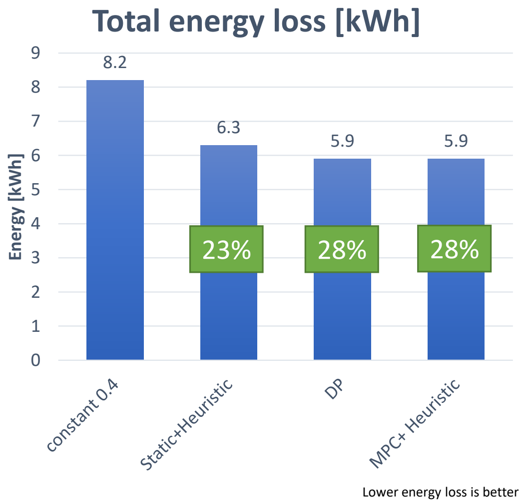

Figure 4.11: Controller comparison high speed highway cycle

The controllers were also compared for two more cycles. A city drive cycle and a highway+city combined drive cycle. Figure 4.12 shows the performance of the four different controllers for the city cycle. This is low thermal load drive cycle and the end winding temperature of both front and rear machine are well within limits. The torque split is mainly governed by power loss and is almost similar for the three dynamic controllers. Figure 4.13 shows an expanded view of the torque split for the three controllers.

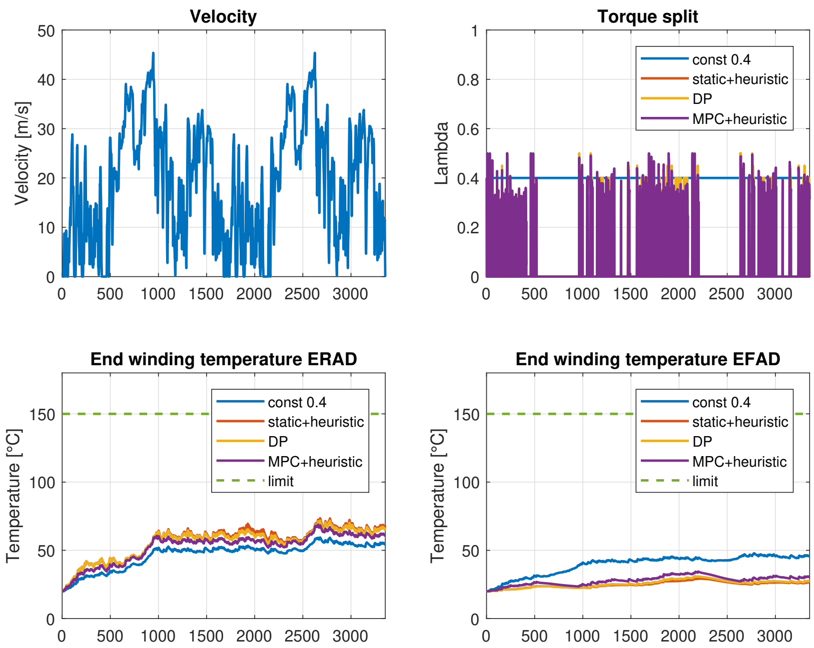

Figure 4.12: Effect of temperature dependent power loss maps

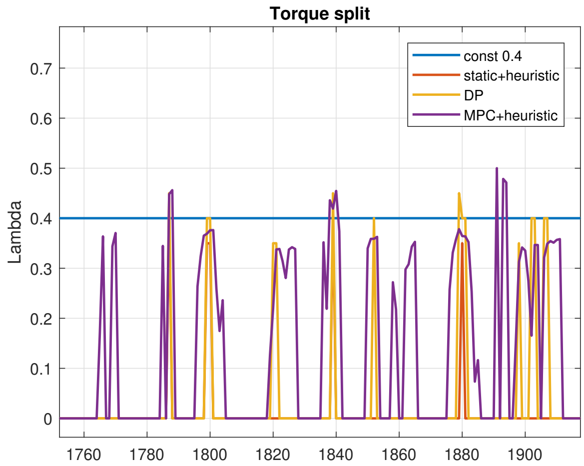

Figure 4.13: Torque split by different controllers for city cycle

The difference in torque split between MPC and DP is attributed to the error associated with fitting a 3D polynomial curve to match the electrical machine power loss which is 5D. The voltage dimension has been reduced by taking the losses at nominal value i.e. @370V. The two temperature dimensions has also been merged to a single dimension which is also an error source. This approximate power loss leads to slightly inefficient controller when compared to static+heuristic and DP as shown in figure 4.14. As the temperature difference between front and rear electric machine is not high, there is not much difference between the static+heuristic and the DP controller.

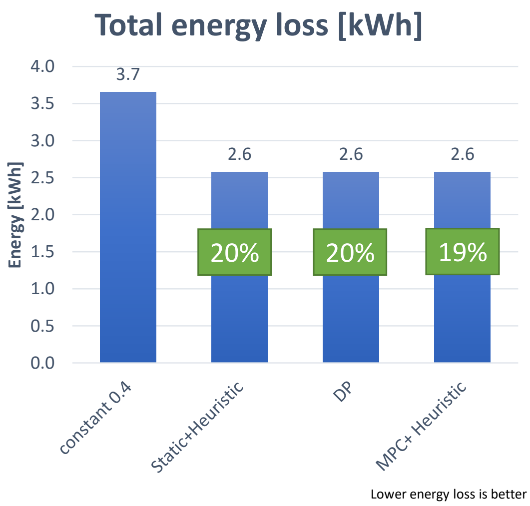

Figure 4.14: Controller comparison city cycle

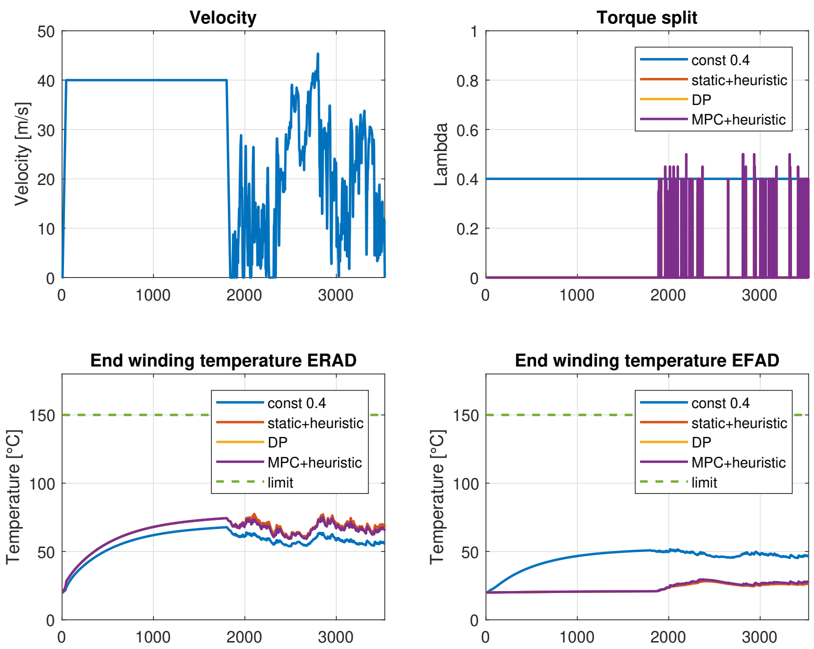

Figure 4.15: Effect of temperature dependent power loss maps

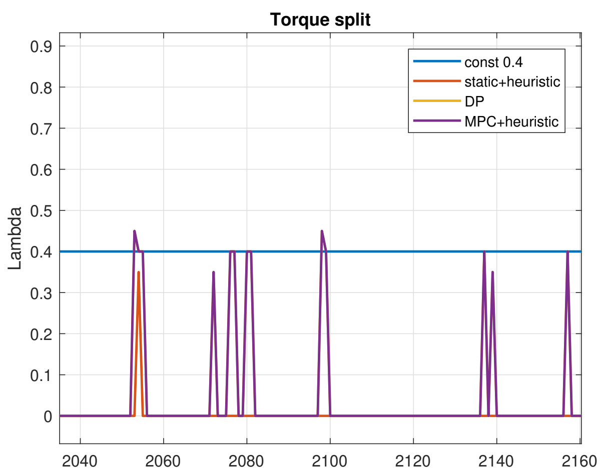

Figure 4.16: Torque split by different controllers for combined highway and city cycle

Figure 4.15 shows the comparison for the four control strategies in a combined highway and city cycle. The vehicle is first driven at constant speed of 40 m/s and then the city cycle is followed. Running at highway speed increases the temperature of the rear electric machine to around $70°C$. This creates a temperature difference between the two electric machines. The battery also gets discharged and at the start of city cycle the voltage is around 370V. The power loss model for MPC and DP becomes similar under these conditions. This effect is easily visible in figure 4.16 where both MPC and DP have same torque splits.

As the static+heuristic controller takes no effect of temperature difference between the machines, it has a different torque split when compared to other two controllers. This has however, no significant effect when comparing energy loss and all the three controllers have same benefit when compared to a constant torque split as shown in figure 4.17.

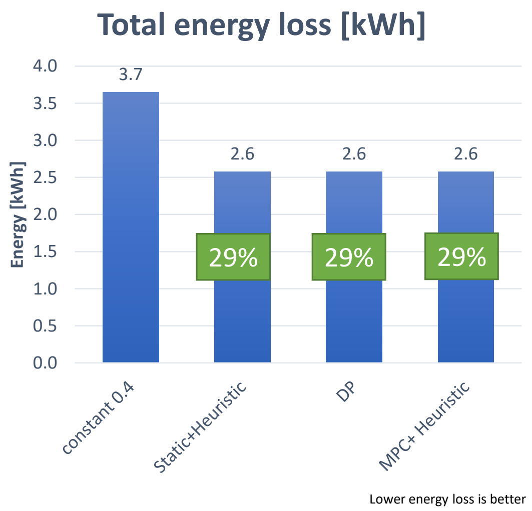

Figure 4.17: Controller comparison for combined highway and city cycle

4.5 Why MPC controller?

MPC and static+heuristic controllers are both online controllers which don't require the drive cycle information to be known beforehand. The MPC controller has the complete thermal dynamic model of the coolant circuit and with a 5 second prediction horizon is computationally expensive. But,the behaviour of both these controllers is quite similar when comparing the energy loss benefit and the thermal performance, except at conditions where temperature is close to limit. So the question is why exactly do we need to have thermal dynamics in the online controller? The answer to this question lies in the fact that the MPC controller is capable of predicting the radiator out temperature among others. The pump speed is usually a function of radiator out temperature and as such MPC can be used to control pump speed also. In cases where the pump losses are significant, this can have a positive effect in the total energy savings. MPC controller is also better in conditions where there is a temperature difference between the two machines and when the component temperature are very close to limit.

4.6 Controller performance for forward plant model

The forward model as explained before does not have a constant torque input but rather has a driver model which calculates the accelerator pedal response. This is

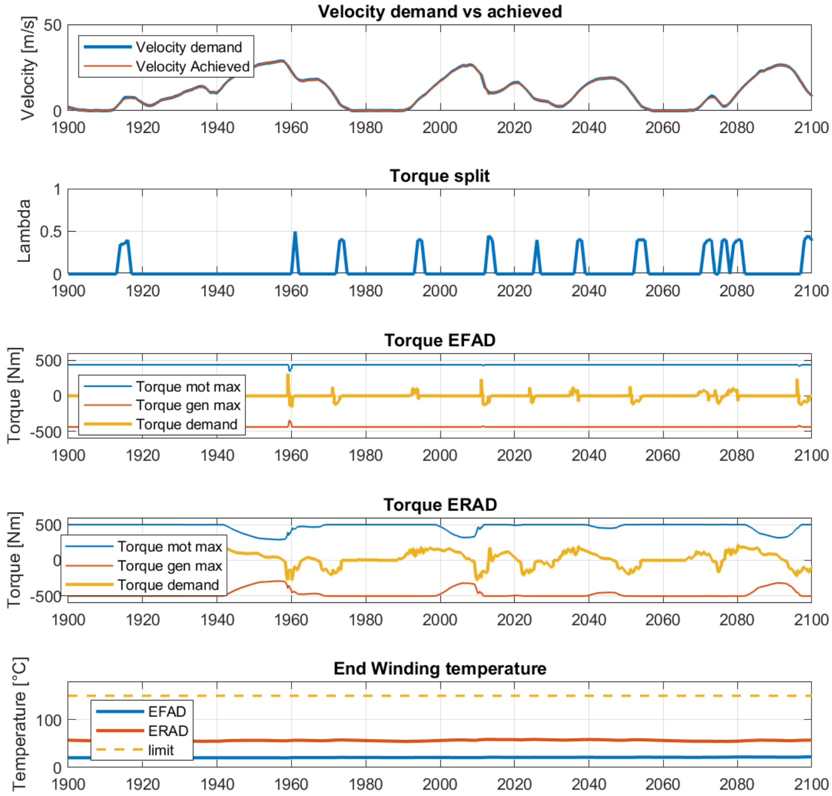

Figure 4.18: Controller performance with forward plant model

done by considering the error between the target and actual velocity. It also models an inverter which has a PID controller for meeting motor speed requirements. As such, it is interesting to see how these controllers performed in this kind of environment. This is also much closer to actual operation of the car. It will be a test for the objective problem formulation as the cost involved during clutch engagement/disengagement was ignored. Figure 4.18 shows the performance of DP controller for a section of the combined highway and city cycle. The driver model is able to meet the target velocity requirement. Whenever lambda changes from 0 to any other value, clutch is engaged and there is positive spike in torque of the front motor. Clutch disengagement similarly has a negative torque spike. With this plant model also, an energy benefit was observed with the three controllers when compared to constant torque split approach. This indicates that the energy saved during clutch disengagement phase is higher than the energy required to dynamically perform clutch actuation process. This still ignores the energy required by the clutch actuator itself. Comparing the different dynamic clutch engagement control strategies, their performance was found very close to each other as shown in figure 4.19. Having almost similar benefit in this type of modelling approach ensures that the controller developed is robust and is able to handle small torque fluctuations,

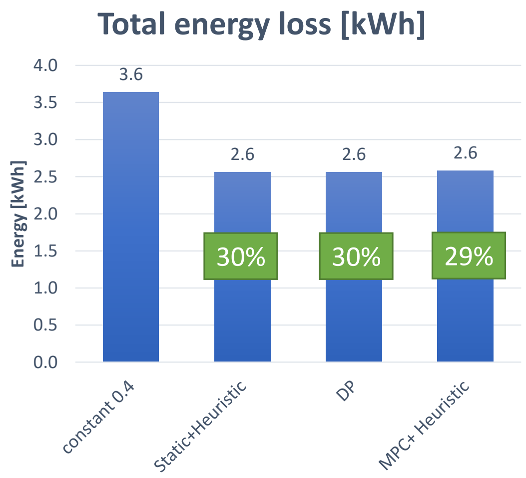

Figure 4.19: Controller comparison with forward plant model for combined highway and city cycle

without affecting the energy savings potential.

5
Conclusion

5.1 Conclusion

One of the main objectives of this thesis was to verify the effect of including thermal dynamics in the optimal torque split strategy for BEV powertrain. For this purpose, control oriented simplified thermal models of the powertrain were created. These simplified models were validated against the high fidelity GT-suite model and predicted temperature within acceptable error bounds. The advantage of simplifying in terms of reduced computation for online controller outweighs the little loss in accuracy for this application.

A static controller spliting torque just based on optimising powerloss without thermal consideration could overuse one of the electric machines, driving its temperature beyond operating limits. It was verified that including thermal dynamics in controller helps restrict the temperature within limits. Since the efficiency of electric machine and inverters vary with temperature, it was also hypothesized that a controller minimizing powerloss should try to operate these components at optimum temperature. But a small benefit of including temperature dependent powerloss maps was observed only in High torque/Low RPM region where copper losses due to high current dominate magnetic drag loss. The benefit observed could be increased if there is a high density of operating points, which fall in between the optimal clutch engagement line at low and high temperatures. The major contribution to energy savings is obtained by disengaging the clutch dynamically whenever torque requirement is less and temperature is within limits.

Two types of online controllers – static + heuristic and MPC + heuristic – were made and verified against the benchmark solution from Dynamic Programming control policy. Both the controllers allowed dynamic torque split and clutch control without exceeding temperature limits. The MPC strategy has added advantage of horizon but requires more computational power and needs a speed and torque prediction as input. A simple static controller can also provide considerable energy savings as compared to a constant torque split strategy.

5.2 Future work

It was concluded that static+heuristic controller performed nicely when the temperature was within limits. Their performance deteriorated close to the penalty limits, and as such different heuristic rules can be tested to have a better controller. As the scope of this thesis has been limited to dynamic controllers, the full benefit that can be achieved by adding heuristic rules to static controller could not be explored.

The simplified thermal model created showed good correlation in normal driving conditions, but had bad results for extreme high speed high torque conditions. A further investigation in this regard can help develop a more robust controller thermal model.

The benefit of including temperature dependent power loss maps was not significant for the powertrain configuration selected. It will be interesting to observe the same with another powertrain configuration having different temperature dependence on loss maps.

The pump loss in the present study was ignored as it was found to be insignificant when comparing to other losses. Looking into the thermal circuit and identifying other sources of losses like energy spent in opening radiator flaps or operating radiator fan which are temperature dependent can potentially increase the benefit of this concept.

The online MPC controller developed here requires online computation with variable time. One of the immediate directions in the future work could be to build an offline optimal controller based on explicit MPC or stochastic dynamic programming. An MPC controller, whether online or offline, requires speed and torque prediction in this case. Since speed and torque prediction based on route navigation and driver behavior is a separate problem in itself, it was out of scope of this study. Hence, another direction for future work could be prediction.

The scope of this study was limited to considering only thermal effects. But the frequency of clutch actuation and torque split also affects NVH (noise-vibration-harness) aspects. Also its important to consider longitudinal dynamic load distribution while determining torque split. Hence, in future study the scope could be expanded to include these domains. Another configuration of interest could be to have clutch on both axles and examine the benefits. This will allow more freedom to the controller and we could see more effect of including temperature dependence of efficiency of components.

Bibliography

[1] S. karlsson and D. Kushnir, "How energy efficient is electrified transport?" in *Systems perspectives on electromobility*, B. Sandén and P. Wallgren, Eds. Göteborg: Chalmers University of Technology, 2017, ch. 5, pp. 49–63.

[2] R. Schmuch, R. Wagner, G. Hörpel, T. Placke, and M. Winter, "Performance and cost of materials for lithium-based rechargeable automotive batteries," *Nature energy*, 2018.

[3] G. Titov and J. A. Lustbader, "Modeling control strategies and range impacts for electric vehicle integrated thermal management systems with matlab/simulink," *SAE Technical Paper*, 2017.

[4] M. Jagiellowicz, M. Hanig, and M. Schmitz, "Development and evaluation of driver coaching function for electric vehicles," Wuerzburg Institute for Traffic Sciences, Tech. Rep.

[5] A. Brahma, "A unified approach to optimal energy management in hybrid vehicles," Master's Thesis, The Ohio State university, 1999.

[6] L. Guzzella and A. Sciarretta, *Vehicle propulsion sytem, An introduction to modelling and optimization,3^{rd}edition. Springer*, 2013.

[7] T. Bengtsson, D. Carlsson, O. Klang, and F. Lier, "Energy optimal power-split control strategy for bevs," 2020.

[8] C. Micallef, "End winding cooling in electric machines," PhD Thesis, University of Nottingham, 2006.

[9] "Thermal design and temperature ratings of igbt modules," ABB, Tech. Rep., 5SYA 2093-00.

[10] V. Cars. Vsim-complete vehicle energy flow simulations. [Online]. Available: https://intranet.volvocars.net/sites/VSim-sp

[11] E. Grunditz, "Design and assessment of battery electric vehicle powertrain, with respect to performance, energy consumption and electric motor thermal capability," PhD thesis, Chalmers University of Technology, 2016.

[12] J. Lindström, "Development of an experimental permanent-magnet motor drive," Licentiate of engineering, Chalmers University of Technology, 1999.

[13] *MATLAB manual*, 2021. [Online]. Available: https://se.mathworks.com/help/ident/gs/about-system-identification.html

[14] H. Sandberg, *Introduction to Model Order Reduction.* KTH Royal Institute of Technology, 2019.

[15] L. S. Simona Onori and G. Rizzoni, *Hybrid electric vehicles, Energy management strategies.* Springer, 2016.

[16] C. E. Garcia, D. M. Prett, and M. Morari, "Model predictive control: Theory and practice—a survey," *Automatica*, vol. 25, no. 3, pp. 335–348, 1989.

[17] MATLAB. Balreal function. [Online]. Available: https://se.mathworks.com/help/control/ref/lti.balreal.html

[18] ——. modred function. [Online]. Available: https://se.mathworks.com/help/control/ref/ss.modred.html

[19] J. A. Andersson, J. Gillis, G. Horn, J. B. Rawlings, and M. Diehl, "Casadi: a software framework for nonlinear optimization and optimal control," *Mathematical Programming Computation*, vol. 11, no. 1, pp. 1–36, 2019.

[20] P. Bonami and J. Lee, "Bonmin user's manual," *Numer Math*, vol. 4, pp. 1–32, 2007.

[21] A. Wächter and L. T. Biegler, "On the implementation of an interior-point filter line-search algorithm for large-scale nonlinear programming," *Mathematical programming*, vol. 106, no. 1, pp. 25–57, 2006.

DEPARTMENT OF ELECTRICAL ENGINEERING
CHALMERS UNIVERSITY OF TECHNOLOGY
Gothenburg, Sweden
www.chalmers.se

CHALMERS
UNIVERSITY OF TECHNOLOGY